NAVAL POSTGRADUATE SCHOOL

MONTEREY, CALIFORNIA

THESIS

NUMERICAL ANALYSIS OF THE PERFORMANCE OF STAGGERED PIN-FIN MICRO HEAT EXCHANGERS

by

Jui Sheng Choo

December 2003

Thesis Advisor: Ashok Gopinath

Approved for public release; distribution is unlimited

THIS PAGE INTENTIONALLY LEFT BLANK

REPORT DOCUMENTATION PAGE			Form Approved OMB No. 0704-0188
Public reporting burden for this collection of information is estimated to average 1 hour per response, including the time for reviewing instruction, searching existing data sources, gathering and maintaining the data needed, and completing and reviewing the collection of information. Send comments regarding this burden estimate or any other aspect of this collection of information, including suggestions for reducing this burden, to Washington headquarters Services, Directorate for Information Operations and Reports, 1215 Jefferson Davis Highway, Suite 1204, Arlington, VA 22202-4302, and to the Office of Management and Budget, Paperwork Reduction Project (0704-0188) Washington DC 20503.			
1. AGENCY USE ONLY ***(Leave blank)***	**2. REPORT DATE** December 2003	**3. REPORT TYPE AND DATES COVERED** Master's Thesis	
4. TITLE AND SUBTITLE: Numerical Analysis of the Performance of Staggered Pin-Fin Micro Heat Exchangers			**5. FUNDING NUMBERS**
6. AUTHOR(S) Jui Sheng Choo			
7. PERFORMING ORGANIZATION NAME(S) AND ADDRESS(ES) Naval Postgraduate School Monterey, CA 93943-5000			**8. PERFORMING ORGANIZATION REPORT NUMBER**
9. SPONSORING /MONITORING AGENCY NAME(S) AND ADDRESS(ES) N/A			**10. SPONSORING/MONITORING AGENCY REPORT NUMBER**
11. SUPPLEMENTARY NOTES The views expressed in this thesis are those of the author and do not reflect the official policy or position of the Department of Defense or the U.S. Government.			
12a. DISTRIBUTION / AVAILABILITY STATEMENT Approved for public release; distribution is unlimited			**12b. DISTRIBUTION CODE**

13. ABSTRACT (maximum 200 words)

The heat transfer and pressure drop characteristics of a staggered micro pin-fin heat exchanger were analyzed using a three dimensional finite element based numerical model. Simulations were conducted based on low Reynolds number, fully developed laminar airflow through an array of circular pin-fins. A range of results was obtained from different configurations with varying pin spacing, axial pitch and pin height. The results from this study would be useful in ongoing work on the design of a laminar flow micro heat exchanger for high heat flux dissipation systems

14. SUBJECT TERMS Numerical Analysis Heat Transfer, Micro Pin-fin Heat Exchanger, Turbine Blade Cooling, Electronic Component Cooling			**15. NUMBER OF PAGES** 103
			16. PRICE CODE
17. SECURITY CLASSIFICATION OF REPORT Unclassified	**18. SECURITY CLASSIFICATION OF THIS PAGE** Unclassified	**19. SECURITY CLASSIFICATION OF ABSTRACT** Unclassified	**20. LIMITATION OF ABSTRACT** UL

NSN 7540-01-280-5500 Standard Form 298 (Rev. 2-89)
Prescribed by ANSI Std. 239-18

THIS PAGE INTENTIONALLY LEFT BLANK

Approved for public release; distribution is unlimited

NUMERICAL ANALYSIS OF THE PERFORMANCE OF STAGGERED PIN-FIN MICRO HEAT EXCHANGERS

Jui Sheng Choo
Captain, Singapore Armed Forces (Army)
B.Eng. (Hons), University of Glasgow, UK, 1998

Submitted in partial fulfillment of the
requirements for the degree of

MASTER OF SCIENCE IN ENGINEERING SCIENCE

from the

NAVAL POSTGRADUATE SCHOOL
December 2003

Author: Jui Sheng Choo

Approved by: Ashok Gopinath
Thesis Advisor

Anthony Healey
Chairman, Department of Mechanical Engineering

THIS PAGE INTENTIONALLY LEFT BLANK

ABSTRACT

The heat transfer and pressure drop characteristics of a staggered micro pin-fin heat exchanger were analyzed using a three dimensional finite element based numerical model. Simulations were conducted based on low Reynolds number, fully developed laminar airflow through an array of circular pin-fins. A range of results was obtained from different configurations with varying pin spacing, axial pitch and pin height. The results from this study would be useful in ongoing work on the design of a laminar flow micro heat exchanger for high heat flux dissipation systems

THIS PAGE INTENTIONALLY LEFT BLANK

TABLE OF CONTENTS

LIST OF FIGURES

THIS PAGE INTENTIONALLY LEFT BLANK

LIST OF TABLES

THIS PAGE INTENTIONALLY LEFT BLANK

NOMENCLATURE

A	area [m^2]
$\overline{A}$	average array flow area [m^2]
Cp	specific heat capacity [J/kgK]
D	pin-fin diameter [m]
D_h	hydraulic diameter [m]
E	fluid friction power per unit area [W/m^2]
f	friction factor
h	heat transfer coefficient [W/m^2K]
H	pin height [m]
k	thermal conductivity [W/mK]
L	array length [m]
$\dot{m}$	mass flow rate [kg/s]
N	number of pin-fin rows
Nu	Nusselt number
P	pressure [Pa]
Q	heat transfer rate [W]
Re	Reynolds number
S	spanwise spacing between pin centers [m]
T	temperature [K]
ΔT_{lm}	log mean temperature difference [K]
U	flow velocity [m/s]
V	volume [m^3]
X	streamwise spacing between centers [m]
ρ	density [kg/m^3]
μ	dynamic viscosity [Pa s]

THIS PAGE INTENTIONALLY LEFT BLANK

ACKNOWLEDGMENTS

Among the many people who helped me through my thesis research, I would like to express my heartfelt gratitude to my thesis supervisor, Professor Ashok Gopinath for his guidance, patience and dedication. I have benefited a lot from his invaluable knowledge and insight. I would also like to thank CDR Hamilton, U.S. Navy for his time and guidance.

Most importantly, I would like to thank my beautiful wife for her love, understanding and support. I am truly grateful for her encouragement and motivation.

THIS PAGE INTENTIONALLY LEFT BLANK

I. INTRODUCTION

A. BACKGROUND/MOTIVATION

Recent advancements in micro technology such as in micro-turbines systems, microelectronic systems, and microelectromechanical systems (MEMS) have spurred the need for the development of high heat flux capable micro heat exchangers. Miniaturizations of mechanical and electronic components lead to higher heat fluxes that can damage or even destroy the components, and hence it is essential to develop efficient and compact heat dissipation devices.

The components of such miniaturized systems may be subjected to adverse heat conditions which can reduce the efficiency of the system, and therefore it is important to enhance their ability to dissipate heat to work safely in the desired operating temperature range. In particular, turbine blades are exposed to an extremely high inlet temperature causing the blade tip to undergo severe thermal stress and fatigue. Hence, effective cooling of the turbines blades is crucial in increasing the turbine performance.

Currently, turbine blade cooling depends primarily on internal forced convection and external film cooling. Convection is through serpentine-ribbed blade coolant passages and external film cooling is provided by injecting air through a series of holes on the blade surface as shown in Figure 1.

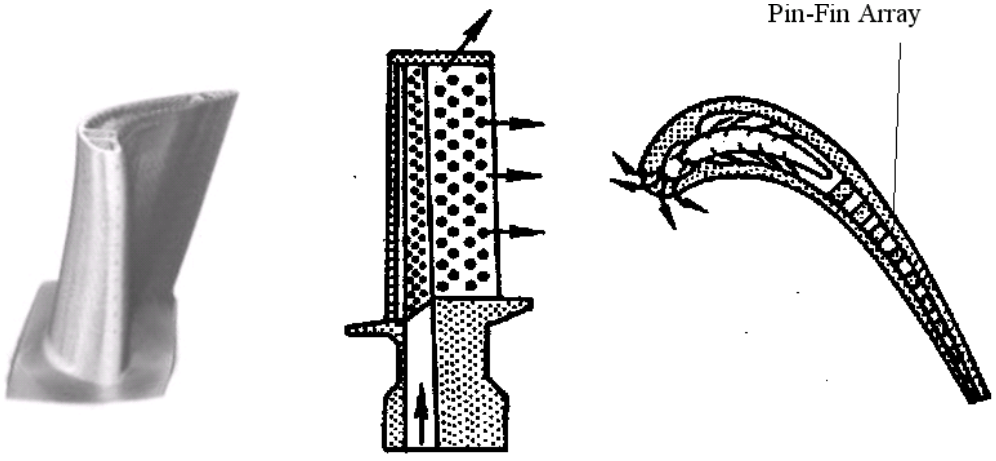

Figure 1 Typical application in a turbine blade

A new concept of increasing the heat transfer from surfaces such as turbine blades has been proposed. The concept is based on electrodepositing a micro heat exchanger directly on the gas turbine component surface. The heat exchanger consists of pin-fins array mounted to the component surface and connected to a shroud (or canopy) as shown in Figure 2. The coolant air is circulated through the pin-fins array between the shroud and original blade surface. This will passively reduce the heat transfer to the microstructure-covered surface and increase allowable turbine inlet temperature.

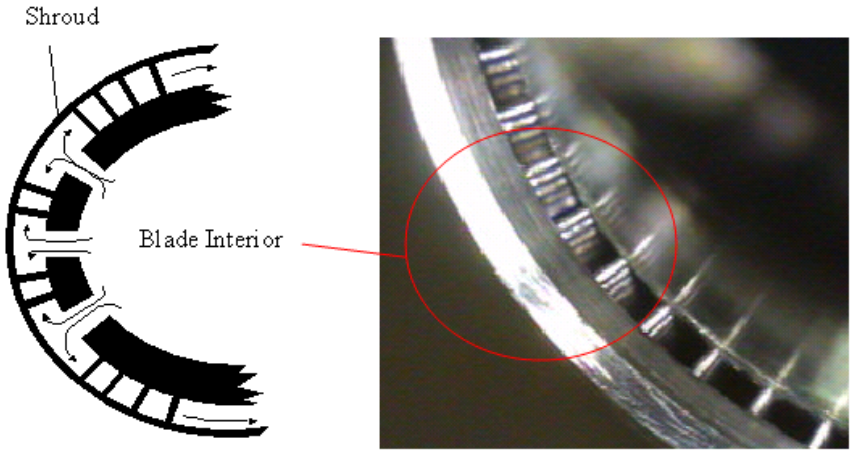

Figure 2 Proposed blade shroud configuration

Typically, a micro heat exchanger is made up of short pin-fin arrays arranged in either staggered or in-line patterns in an internal flow passage or duct. The microscopic view of a micro heat exchanger array can be seen in Figure 3. Coolant is injected into the flow passage perpendicular to the cylindrical solid pins. The array dimensions may be defined by pin diameter (D), pin height (H), streamwise pin spacing (X) and spanwise pin spacing (S) as shown in Figure 4. Pins may be categorized as short if the ratio H/D is on the order of unity, which is the primary focus of this study.

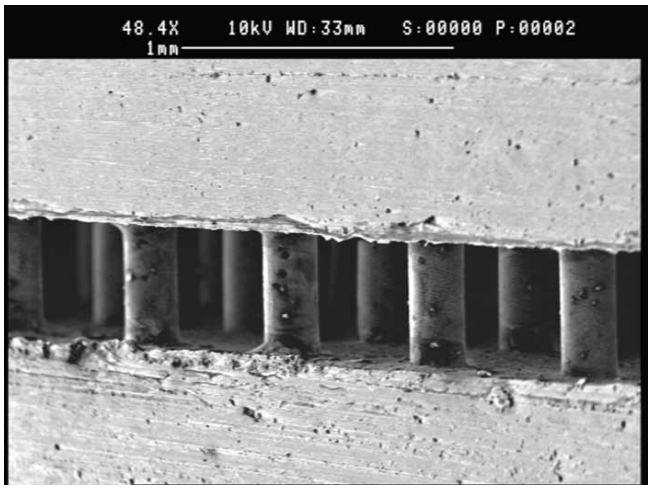

Figure 3 A microscopic pin-fin array

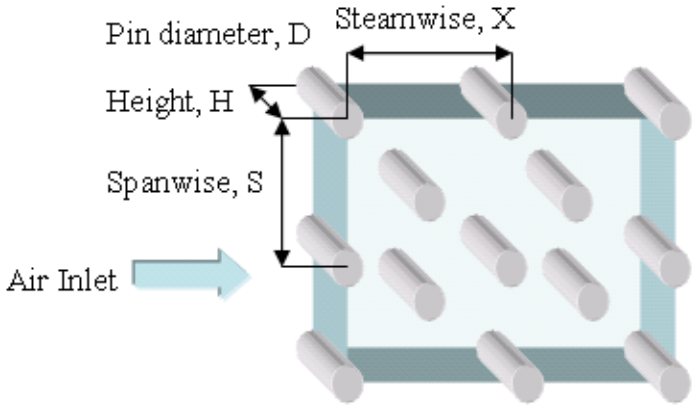

Figure 4 Schematic of a staggered pin-fin array

B. PREVIOUS WORK

Empirical studies have been carried out extensively over the years on macroscale pin-fin heat exchangers to determine their heat transfer characteristics in order to enhance their performance. Van Fossen (Ref. 1) early work was based on staggered pin-fins array for *H/D* values of 0.5 and 2.0 with Reynolds number varying from 300 to nearly 60000. He discovered that the heat transfer coefficient for short pins to be lower than longer pins. Sparrow et al. (Ref. 2) later examined the heat transfer behavior for cylinder adjacent to the endwall and discovered that heat transfer was lower at the wall as compared to the regions of the cylinder away from the wall. Chyu, et al. (Ref. 3) also determined that the

heat transfer coefficient on the pin surface was 10 to 20 percent higher than the uncovered endwall.

Metzger, et al. (Ref. 4) conducted an empirical study to investigate the streamwise row-averaged heat transfer coefficients for a staggered short pin-fin array. He used a two ten-row arrangements with H/D=1.0, S/D=2.5 and X/D=1.5 and 2.5 for Reynolds number spanning of approximately 10^3 to 10^5. They found that the heat transfer coefficient peaked between the third and fifth row of the array.

Donahoo, et al. (Ref. 5) conducted a numerical study on the optimization using a general-purpose viscous flow solver to simulate the flow through a staggered pin-fin array and the effect of heat transfer. The simulation was based on a 2-D only model to examine the tumultuous flow characteristics around the pins and near wall regions. Their results were consistent with the findings of Metzger et al. findings, and demonstrated that the maximum heat transfer coefficient occurs between row four and five although being 2-D in nature were unable to capture the pin-end wall interaction effects.

Hamilton (Ref. 6) conducted a numerical analysis on the heat transfer characteristics on various staggered short pin-fin array heat exchangers. He demonstrated that a suitably defined hydraulic diameter could be used as a characteristic length scale. He found that the reduction in axial pitch could produce a significant increase in heat exchanger performance. Another finding was that small increases in heat transfer coefficient resulted in disproportionately large increases in frictional losses. He suggested that the results of macroscale experiments could be directly applied to microscale heat exchanger.

However, these studies have all been based on macroscale heat exchanger designs and at high Reynolds numbers. After an extensive search, there were no articles found contributing to the study on the heat transfer characteristics and performance of a laminar flow microscale pin-fin array heat exchanger. Since the length scales of a microscale pin-fin array are dramatically smaller, the conventional thinking derived from large sized heat exchangers will no doubt undergo a paradigm change.

C. OBJECTIVES

An extensive search of the literature has revealed that there is a lack of three dimensional numerical simulation models for the analysis of low Reynolds number laminar flow and heat transfer through a staggered short pin-fin micro heat exchanger. Experiments are normally labor intensive and expensive to conduct and it would be wise to perform numerical analyses along with devising an experimental strategy. The major goal of this study is to develop a three dimensional numerical model of the staggered short pin-fin micro heat exchanger to examine its heat transfer and pressure drop characteristics for various configurations of laminar flow. This model will be used to examine the effects of axial pitch, spanwise pitch, and height of the pins on the performance of the heat exchanger. The numerical solution will also be used to deduce an optimal configuration for the heat exchanger.

D. METHODOLOGY

A three-dimensional numerical pin-fin array model was constructed using the commercial finite element analysis package ANSYS. This numerical model was then used to perform simulation on various configurations based on a carefully defined test matrix. The numerical solution was then evaluated and the details will be discussed in the following section.

THIS PAGE INTENTIONALLY LEFT BLANK

II. NUMERICAL ANALYSIS

A. FINITE ELEMENT MODELING

1. Modeling

A commercial finite element analysis package ANSYS (Version 7.1) was selected to generate a three-dimensional micro heat exchanger and perform numerical analysis on the model. The finite element models were constructed using ANSYS PREP7 and the model data was passed to the FLOTRAN CFD (Computational Fluid Dynamics) module for various analyses. FLOTRAN CFD is incorporated in ANSYS for solving three-dimensional fluid flow fields in conjugate heat transfer problems. The governing equations solved by FLOTRAN are the Navier-Stokes equations combined with the continuity equation, the thermal transport equation, and constitutive property relationships. Once the FLOTRAN analyses are completed, the data can be transferred to the ANSYS postprocessor.

Typically, a micro heat exchanger has moderately dense array of microstructures coupled between the shroud or canopy and the original surface of the component. Depending upon the spacing and density, the field of microstructures can be used to passively enhance or reduce heat transfer to the microstructure-covered surface. Micro heat exchangers typically have large feature densities consisting of many pins per row and contributions from the sidewalls would make up but a very small fraction of the total flow solution. This behavior may be demonstrated by having finite pin height and infinite span.

Several assumptions were made to simplify the model in order to reduce the computational requirements. Firstly, an infinite span condition was assumed in the spanwise direction and was numerically achieved by taking advantage of the symmetry plane. Further simplification was to model only one quarter of the micro heat exchanger as shown in Figure 5. Secondly, the heat exchanger surfaces were all treated as isothermal by neglecting temperature gradients inside the solids and the resulting boundary conditions are illustrated in Figure 6.

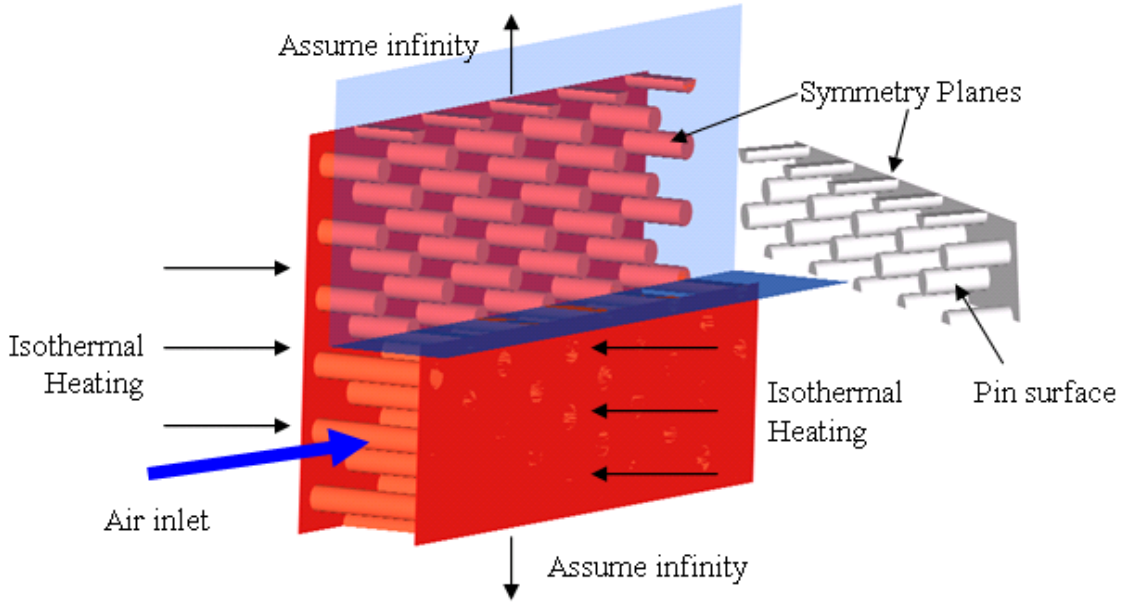

Figure 5 Numerical model details

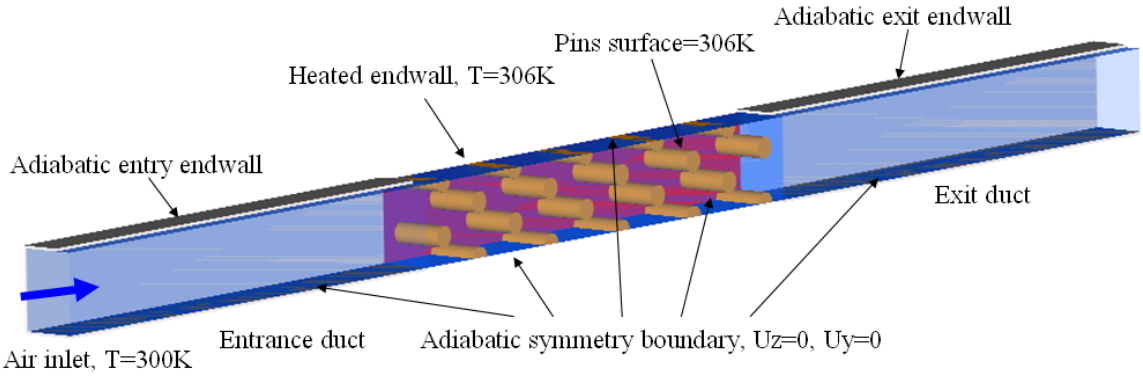

Figure 6 Boundary conditions

The macro tool is a useful feature of ANSYS that has been exploited to ensure consistency and efficiency. The macro tool was used to generate the 3-D model and perform numerical simulations using predefined solutions and iterations. Parameters such as Reynolds number, pin diameter, spanwise ratio, height ratio and boundary conditions were defined in the macro prior to each simulation. The macro tool was also used to specify the mesh density in order to achieve a well-meshed model for each simulation. The mesh density was adjusted to concentrate finer mesh girds around the pins. Thermal gradients are often extremely high near thermal boundaries and therefore,

the mesh should usually be denser near thermal boundaries and finer girds were concentrated around the pins as shown in Figure 7. The analytical outlet bulk temperature was used to check the computational result to ensure that the model was adequately meshed. A sample macro is provided in Appendix A.

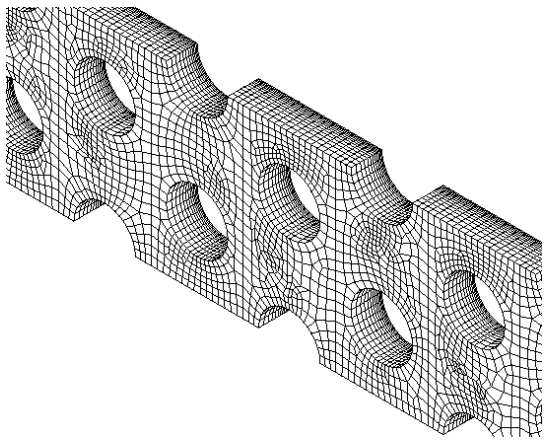

Figure 7 Sample model meshing

An entrance duct was constructed in front of the heat exchanger array test section to ensure a fully developed laminar flow condition at the entrance to the test section. An exit duct was also used to ensure well-mixed conditions at the exit plane. Both the entrance and exit duct are assumed to be adiabatic. Only the endwall of the test section and pin surfaces were maintained at a specified temperature. The no-slip condition has been defined at all fluid-wall boundaries. The velocity component and heat fluxes normal to the boundary of the symmetry planes were set to zero. The velocity was determined from the desired Reynolds number setting for the simulation. A steady-state thermal analysis was used to determine the temperature distribution and other thermal quantities under steady-state loading conditions.

2. Solution Technique

The FLOTRAN CFD solver was used to solve for the flow and temperature distributions within a region. For the FLOTRAN CFD elements, the velocities are obtained from the conservation of momentum principle, the pressure is obtained from the conservation of mass principle, and the temperature is obtained from the law of

conservation of energy. A segregated sequential solver algorithm is used to solve the matrix system derived from the finite element discretization of the governing equation for each degree of freedom. The Preconditioned Generalized Minimum Residual (PGMR) has a tight convergence criterion and is suited for solving the energy equation for ill-conditioned conjugate heat transfer problems. Although PGMR is robust, it is also memory-intensive. The Preconditioned BiCGStab method (PBCGM) was selected for solving the pressure equation for incompressible flow and extremely ill-conditioned conjugate temperature heat transfer problems. The Tri-Diagonal Matrix Algorithm (TDMA) was used for the momentum equations since exact solutions are not required.

The flow problem is nonlinear and the governing equations are coupled together to obtain a final solution. In FLOTRAN, the nonlinear coupling is handled in a segregated manner and the coupling algorithms belong to a general class referred to as the Semi-Implicit Method for Pressure Linked Equations (SIMPLE).

The advection term is crucial in solving the momentum, energy, species transport, or the pressure equations especially when this term dominates over the other terms in these governing equations. It may lead to numerical instabilities if this term is not properly discretized. The Monotone Streamline Upwind (MSU) approach MSU tends to be first order accurate while Collocated-Galerkin (COLG) is second order accurate. MSU produces diagonally dominant matrices and is generally quite robust. COLG provide less diagonal dominance, but are generally more accurate. COLG also provides an exact energy balance for incompressible flows.

FLUID142 was selected to model the steady state fluid/thermal systems. For an ideal gas, the density is calculated from an equation of state involving the absolute pressure and the absolute temperature. Hence, it is crucial to prevent negative pressure and static temperature from being encountered during the iterative process as this would lead to a negative density. For a conjugate heat transfer problem, a converged incompressible pressure solution is desired initially so that the resulting pressures could be used to update the velocities and ensure conservation of mass. Hence, in order to improve the accuracy of the numerical results, the solution for each simulation was segregated into 3 phases. For the initial solution, no thermal analysis was conducted and the density was held constant. This allows the momentum equations to generate the flow

solution. Once the initial series of iterations were completed, the density was allowed to vary in the second phase to in order to solve the energy equation. In the final phase, COLG was used to replace MSU to discretize the advection term.

According to the ANSYS documentation (Ref. 7) the ratio of effective viscosity to laminar viscosity can be used to decide if laminar or turbulence modeling should be used. The documentation recommends that a laminar solution should be used in cases where the laminar viscosity is 5 times greater then the effective viscosity. Hamilton (Ref. 6) showed that this condition was met near a Reynolds number of about 1000, and recommended that laminar modeling be used for Reynolds numbers below 1000.

3. Test Approach

a. Model Validation

Several checks were performed in order to verify the results generated by ANSYS. Threeorders of magnitude of convergence was maintained for each solution in order to ensure accuracy of the results. The contour plots for velocity, temperature and pressure were observed separately to ensure that the results satisfy the boundary conditions.

The result summary file (Jobname.PFL) generated by ANSYS upon completion of each run was carefully examined and analyzed. The conservation of mass was verified by comparing the inlet and outlet mass flow rate to ensure that the mass balance is achieved. The energy flow into and out of the system at the flow boundaries were ensured to be equal to the total energy added at the end wall. Specified wall temperatures and specified film coefficient boundaries were compared to the temperature gradient. If there was a discrepancy in the temperature of more than 0.1 K, the simulation was repeated with either reducing the mesh density of the model and/or increasing the number of solver iterations.

As the dimensions of the micro heat exchanger are small, computational errors both in pressure drop and heat transfer measurements were commonly encountered. This could result in a diverging solution and was corrected by increasing the reference pressure and/or relaxing the modified inertia criteria.

b. Array Characteristic Length

The characteristic length was based on the ratio of open volume (V_{open}) available for fluid flow in the array, to the total fluid wetted area (A_w) and is defined as:

$$D_h = \frac{4V_{open}}{A_w} \qquad (1)$$

This is the same characteristic length used by VanFossen (Ref. 1) and Hamilton (Ref. 6) that is found to collapse all the dimensional data consistently into its non-dimensional form.

c. Entry Length

If significant gradients are calculated near a boundary, a mass imbalance could occur. This is due to the implied condition of fully developed flow for a constant pressure boundary. If the flow has not fully developed, FLOTRAN is forced to adjust it across the last row of elements to satisfy the boundary condition. This adjustment may cause a mass imbalance and can be prevented by adding a development length to the test section. For laminar flow, this length can be calculated using the characteristic length, D_h:

$$\frac{L_e}{D_h} \approx 0.06\,Re_{D_h}$$

$$L_e \approx 0.06\left(D_h\right)\left(Re_{D_h}\right) \qquad (2)$$

d. Reynolds Number

The Reynolds number is defined in terms of the properties of the fluid, characteristic velocity, and characteristic dimension. The Reynolds numbers for flows in the micro heat exchanger are generally very low as the flow velocity in these scaled down hydraulic diameter passages is quite small. Using the revised definition of the characteristic length scale in Eq. (1), the Reynolds number is now defined as:

$$Re_{D_h} = \frac{\rho \bar{U} D_h}{\mu} \qquad (3)$$

where

$$\bar{U} = \frac{\dot{m}}{\rho \bar{A}}$$

and

$$\bar{A} = \frac{V_{open}}{L}$$

e. Test Matrix

A range of studies was conducted based on the three-dimensional model of a staggered short pin-fin micro heat exchanger. The pins diameter for all computation simulations was maintained at 100 μm with varying axial pitch ratio, *X/D*, spanwise ratio, *S/D*, and pin height, *H/D*. While examining the effect of *X/D* and *S/D*, *H/D* was kept constant at a value of 1.0. Table 1 shows the test matrix that was used.

Table 1. Test configurations, baseline numerical circular pin study

Variable	Values
Re_{Dh}	100 – 1,000
S/D	1.25, 1.5, 2.0, 3.0
X/D	1.25, 1.5, 2.0, 3.0
H/D	1.0, 1.5, 2.0, 3.0

4. Data Analysis

Crucial results like total heat transfer rate, inlet and outlet bulk temperature, pressure drop and mass flow rate were obtained from the FLOTRAN output file. The Nusselt number and friction factor of the pin-fins array were calculated using heat transfer relationships.

A simple calculation of the outlet bulk temperature based on the energy balance was performed to verify the result obtained directly from ANSYS. The outlet bulk temperature based on energy balance was determined as follows:

$$T_{bulk,out} = T_{bulk,in} + \frac{Q}{\dot{m}\, C_p} \qquad (4)$$

a. Nusselt Number Calculations

The Nusselt number gives the ratio of actual heat transferred of the pin-fins array by a moving fluid to the equivalent heat transfer that would occur by conduction. The Nusselt number for the was defined as:

$$Nu_{D_h} = \frac{\bar{h}_{array} D_h}{k} \qquad (5)$$

where the heat transfer coefficient

$$\bar{h}_{array} = \frac{Q}{A_{wetted}\ \Delta T_{lm}} \qquad (6)$$

and the log mean temperature difference

$$\Delta T_{lm} = \frac{\left(T_{wall} - T_{bulk,in}\right) - \left(T_{wall} - T_{bulk,out}\right)}{\ln\left(\frac{T_{wall} - T_{bulk,in}}{T_{wall} - T_{bulk,out}}\right)} \qquad (7)$$

b. Friction Factor Calculation

The friction factor in the array was calculated using the following definition:

$$f = \frac{\Delta P_{array} D_h}{\frac{1}{2}\rho \bar{U}^2 L} \qquad (8)$$

where L is the overall streamwise length of the array.

c. Specific Fluid Friction Power

Based on Kays and London (Ref. 8), the heat exchanger performance can be evaluated by plotting the heat transfer coefficient against the friction power. The specific fluid friction power used in this report is defined as:

$$E = \frac{\dot{m}\Delta P_{array}}{\rho_{film} A_{wetted}} \qquad (9)$$

and is a measure of the power expended for pumping the fluid per unit wetted (heat transfer) area.

THIS PAGE INTENTIONALLY LEFT BLANK

III. RESULTS AND DISCUSSION

A. EFFECTS OF AXIAL PITCH

Studies based on macroscale experimental and numerical results have shown that reducing axial pitch would increase area density and therefore has the potential to improve heat exchanger performance. This section will investigate the effects of axial pitch variation.

1. Test Approach

1 The previously defined numerical model was used to study the staggered short pin-fin heat exchanger for various configurations and Reynolds numbers. For this study, the configuration was fixed at *S/D*=1.5 and *H/D*=1. A range of Reynolds numbers from 100 to 1000 were used for this laminar flow model. Figure 8 illustrates the physical effect of the *X/D* ratio for the extreme cases.

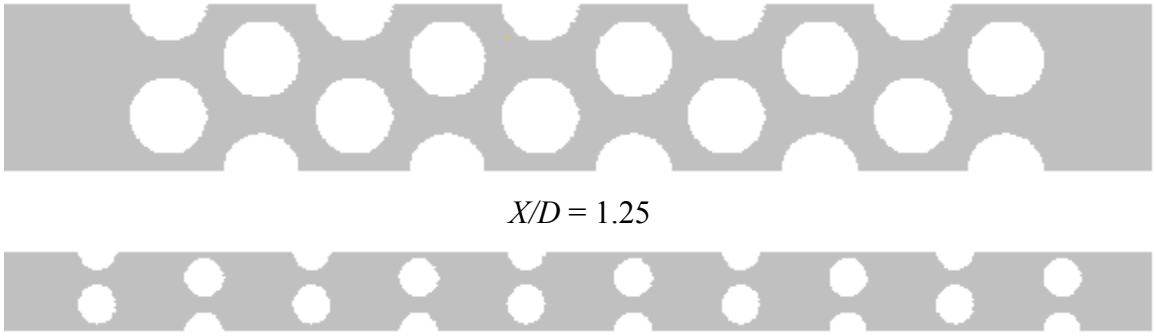

X/D = 1.25

X/D = 3

Figure 8 Physical effect of *X/D*

2. Results and Discussion

a. Effects on Nusselt Number

From the numerical results obtained, the dimensionless Nusselt number was calculated for each test configuration. Figure 9 shows the Nusselt number plotted against Reynolds number on a logarithmic scale for specific *X/D* configurations. In fact,

the figure shows that the Nusselt number increases proportionally with Reynolds number. and all the configurations demonstrate similar characteristics and trends. It was observed from the figure that the Nusselt number was insensitive to *X/D* ratios smaller then 2 for a given a specific Reynolds number.

The slight increase in Nusselt number with reducing *X/D* may be explained by the fact that the Nusselt number depends on both the heat transfer coefficient and hydraulic diameter. The increase in *X/D* causes the hydraulic diameter to increase but it was noticed that the heat transfer coefficient was lower for larger *X/D* values. The rate of increase in hydraulic diameter dominates the reducing rate of heat transfer resulting in an overall increase in Nusselt number. Figure 10 further illustrates only a slight decrease in Nusselt number with increasing axial pitch. This demonstrated that the variation in axial pitch had minimal effects on the Nusselt Number.

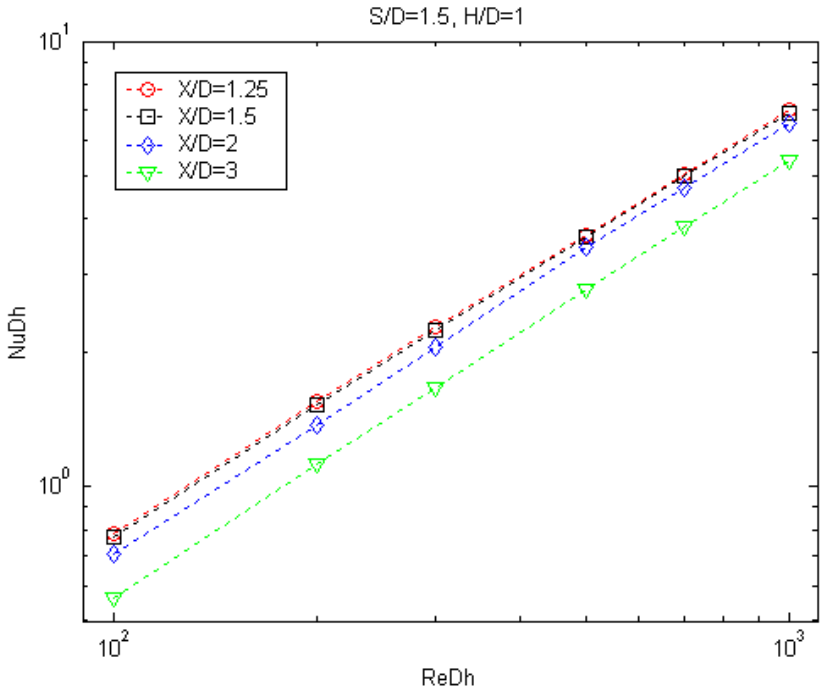

Figure 9 Effect Reynolds number on Nusselt number

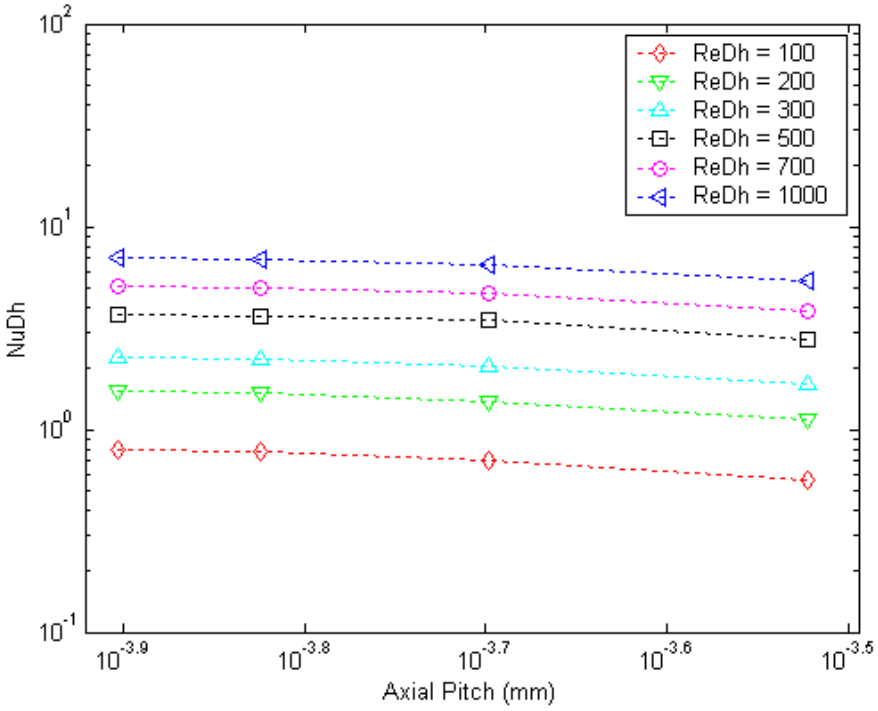

Figure 10 Effect of axial pitch on Nusselt number

b. Effects on Friction Factor

The friction factors and pressure gradients were found to be quite high for flow in a micro heat exchanger since the available surface area for a given flow volume is high. Figure 11 shows the friction factor plotted against Reynolds number on a logarithmic scale for all *X/D* configurations. It is observed that the friction factor drops off with increasing Reynolds number. This behavior is due to the longer overall array length resulting in higher resistance to the flow negotiating through the heat exchanger creating an increase in pressure drop. The effect of axial pitch variation on friction factor is shown in Figure 12. The friction factor was noticed to decrease with reducing axial pitch.

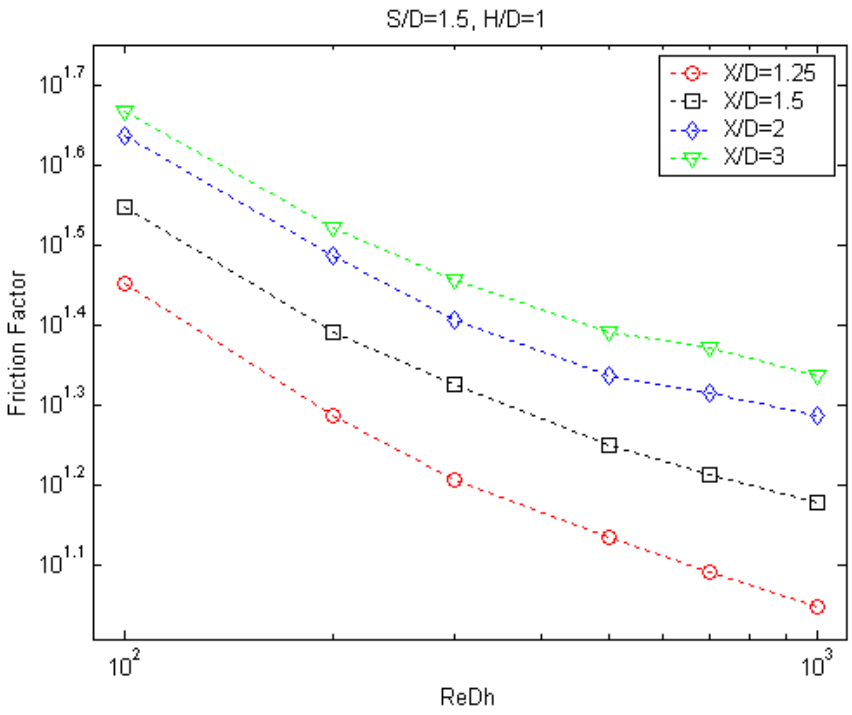

Figure 11 Effect of Reynolds number on friction factor

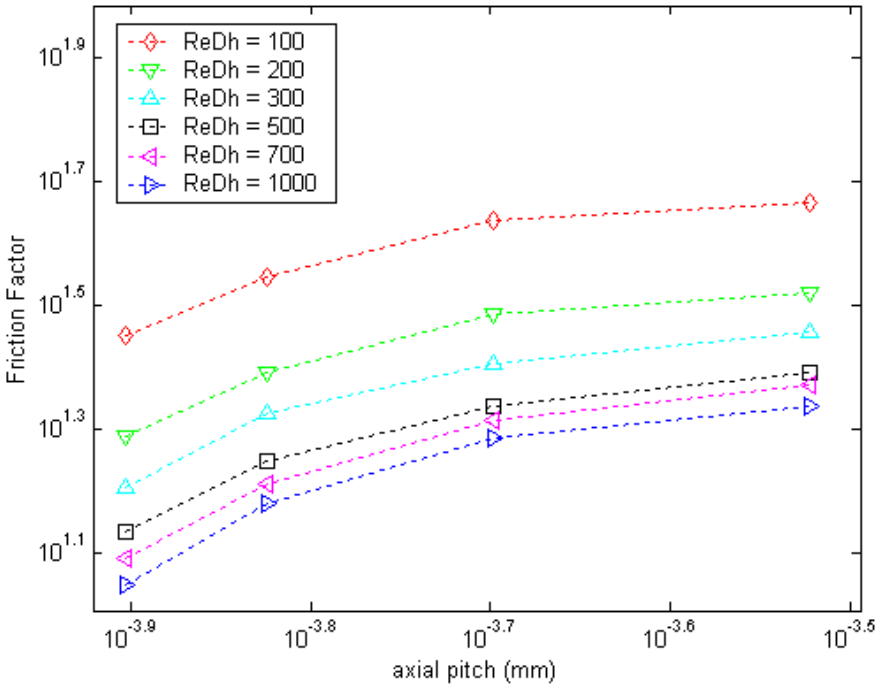

Figure 12 Effect of axial pitch on friction factor

c. Heat Transfer Coefficient

Figure 13 shows the effect of Reynolds number on the heat transfer coefficient for *X/D*=1.25 configurations. Although it is expected that the Reynolds number would strongly influence the heat transfer coefficient, the plots below illustrate the magnitude of this relationship. As defined earlier, the hydraulic diameter was based on the ratio of open volume (V_{open}) available for fluid flow in the array, to the total fluid wetted area. As the axial pitch was decreased, the inlet velocity was increased to maintain the desired Reynolds number due to the smaller hydraulic diameter values. Therefore, the greater flow velocities result in increased heat transfer coefficients. As shown in Figure 14, the heat transfer rate was much greater for ReDh=1000 than for ReDh=100. It may be noted in Figure 14 that the lighter shades represent higher heat transfer rates.

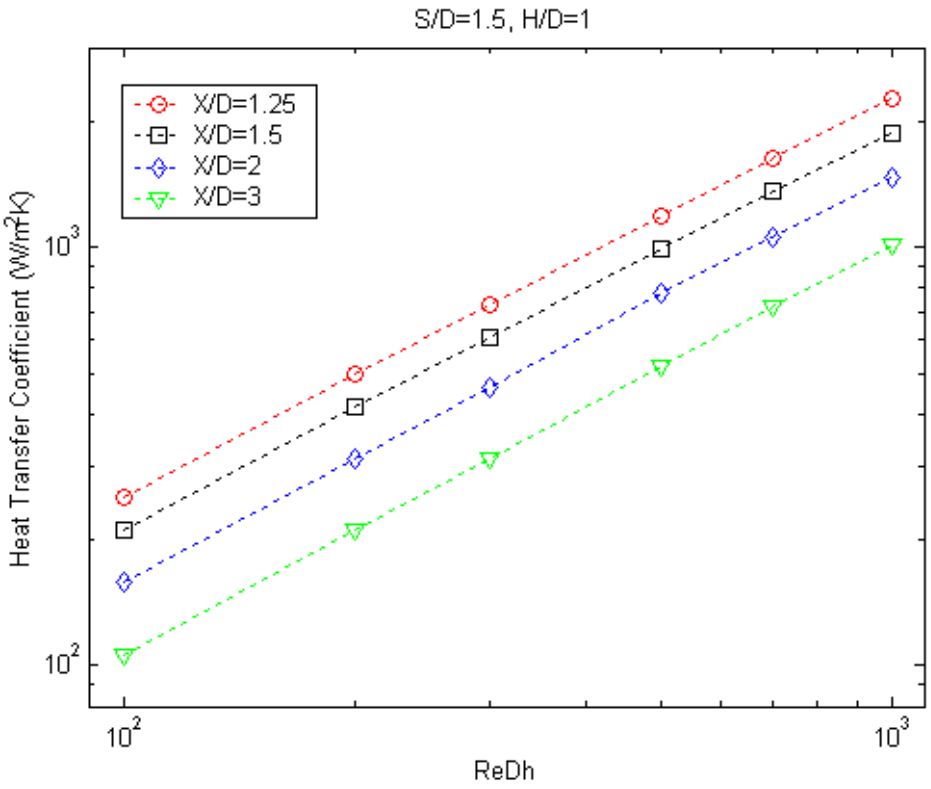

Figure 13 Effect of Reynolds number on heat transfer coefficient

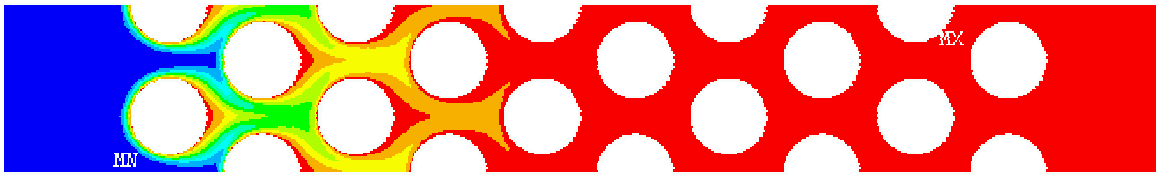

Re=100, *X/D*=1.25, *S/D*=1.5

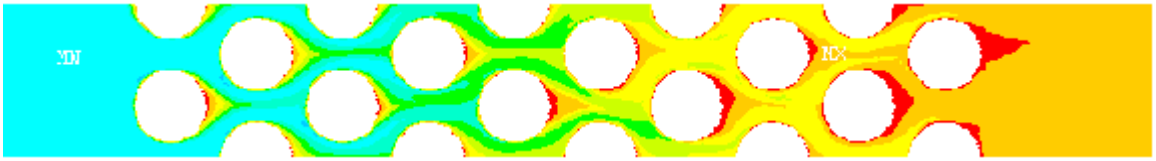

Re=1000, *X/D*=1.25, *S/D*=1.5

Figure 14 Contour plot of heat transfer rate for various Reynolds number

It was also observed that axial pitch variation does have an effect in enhancing the heat transfer coefficient as demonstrated in Figure 15. The contour plot of the heat transfer rate is shown in Figure 16.

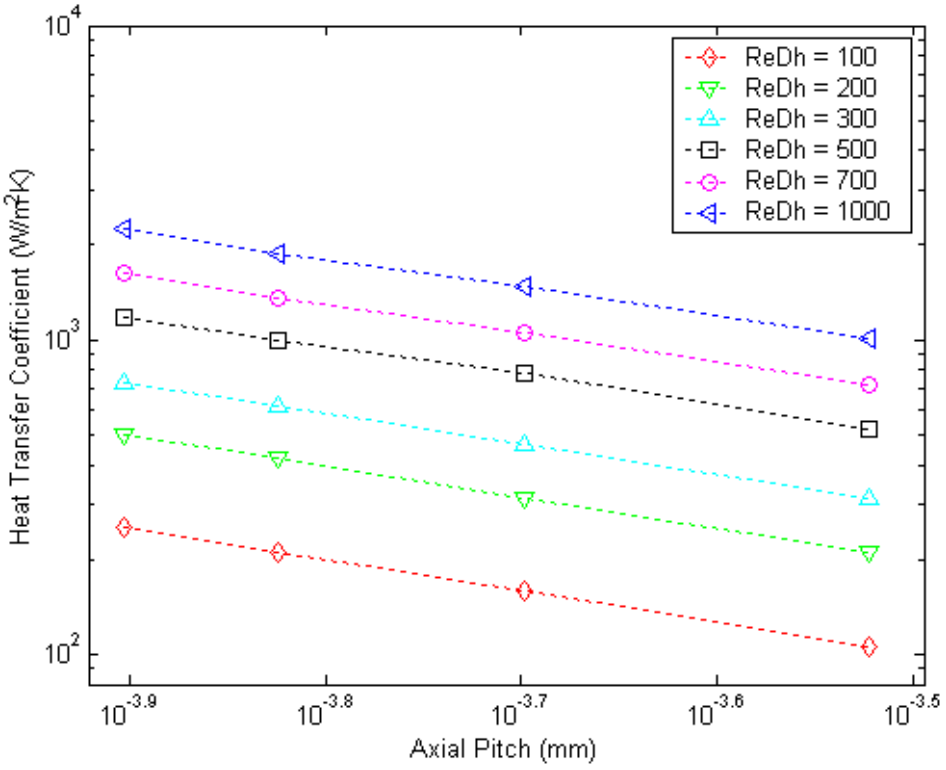

Figure 15 Effect of axial pitch on heat transfer coefficient

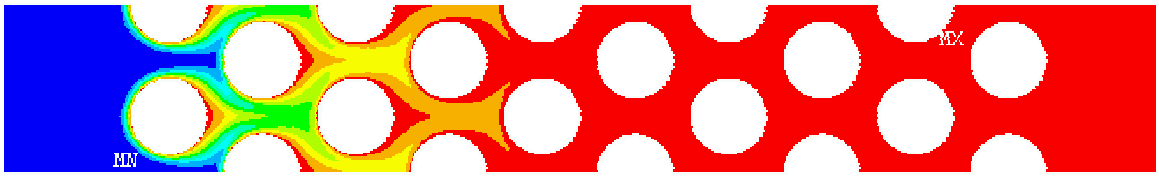

Re=100, *X/D*=1.25, *S/D*=1.5

Re=100, *X/D*=3.0, *S/D*=1.5

Figure 16 Contour plots of heat transfer coefficient for various *X/D*

d. Performance Comparisons

The optimal heat exchanger design configuration was predicted by comparing the heat transfer coefficient with friction power as shown in Figure 17. The ideal design configuration would maximize the heat transfer rate while minimizing frictional losses in the flow. It was found that the most favorable configuration for constant *S/D*=1.5 and *H/D*=1 was for *X/D*=1.25, while the least desirable was for *X/D*=3. This was determined by comparing a specific heat transfer coefficient with the friction power required for each configuration. For example, *X/D*=3 required Re_{Dh}= 1000 and friction power of 5000 W/m^2 to achieve a heat transfer coefficient of 1000 W/m^{2}K, as compared to *X/D*=1.25 which requires approximately Re_{Dh}= 400 and friction power of 1000 W/m^2 to achieve the same heat transfer coefficient. It clearly shows that the least efficient configuration requires 5 times more friction power for the same heat transfer coefficient. It may be concluded that it is more cost effective to enhance heat transfer coefficient through reductions in axial pitch rather than through increase in Reynolds number.

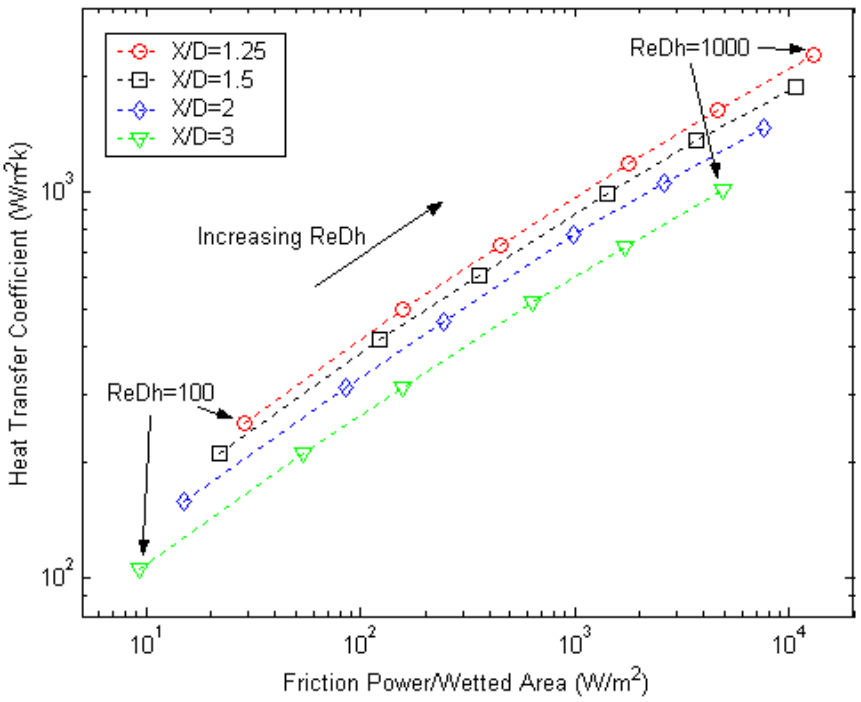

Figure 17 Effect of axial pitch on performance

It was apparent that the effectiveness of the desired configuration was relative to the volumetric density of available heat transfer surface area. The effect of axial pitch on area density, $\frac{A_{wetted}}{Volume}$ can be observed from Figure 18. It shows that the heat exchanger area density increases significantly with reducing axial pitch which is the desired behavior.

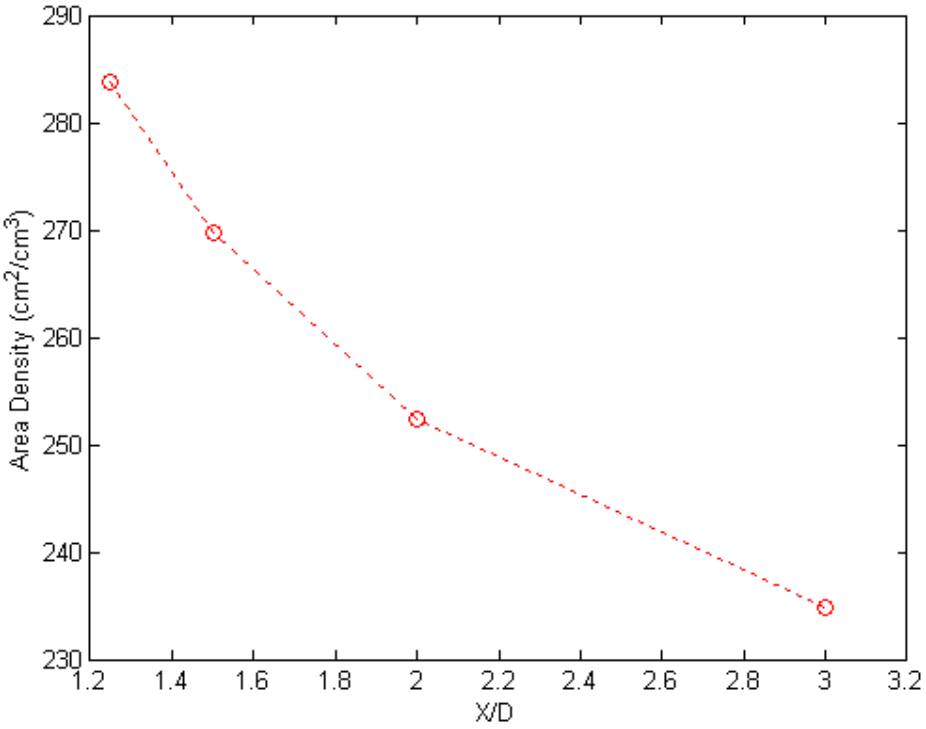

Figure 18 Axial pitch effect on area density

THIS PAGE INTENTIONALLY LEFT BLANK

B. CIRCULAR PINS, EFFECTS OF SPANWISE RATIO

Reducing the spanwise distance between pins would increase area density and similar to decreasing the axial pitch, has the potential to enhance the heat exchanger performance. This section will discuss the effect of spanwise ratio on circular pin-fin heat exchanger performance.

1. Test Approach

An identical numerical model discussed in the previous section was used to study the effect of spanwise distance variation for various configurations and Reynolds numbers. In this section, the configuration was fixed at S/D=1.5 and H/D=1. The Reynolds number was allowed to vary from 100 to 1000 for each S/D configuration. Figure 19 shows the physical effect of the S/D ratio for the extreme cases.

S/D = 1.5

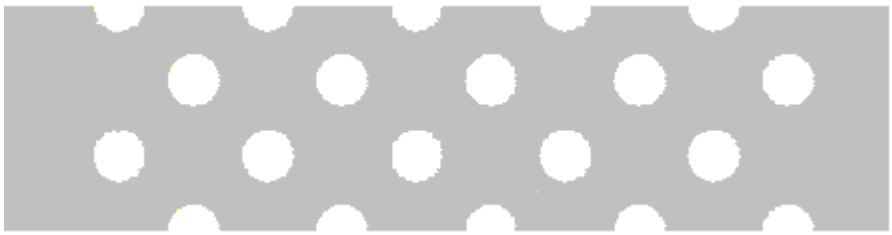

S/D = 3

Figure 19 Physical effect of the *S/D* variation

2. Results and Discussion

a. Effects of Nusselt Number

Figure 20 is a plot of the Nusselt number against Reynolds number on a logarithmic scale for specific *S/D* configurations and shows that all configurations demonstrate similar characteristics and trends. The Nusselt number was observed to

decrease with reducing *S/D* ratio. The figure displayed a similar phenomenon as in *X/D* where the Nusselt number increases proportionally with Reynolds number.

As discussed in the preceding section for *X/D*, the Nusselt number is a function of heat transfer coefficient and hydraulic diameter. The increase in *S/D* caused the hydraulic diameter to increase but it was noticed that the heat transfer coefficient was lower for larger *S/D* values. Therefore, it was apparent that the rate of reduction in heat transfer coefficient was offset by the increasing hydraulic diameter resulting in the increase in Nusselt number. The effect of axial pitch variation on Nusselt number is shown in Figure 21. The Nusselt number showed a slight amplification with increasing spanwise distance but the variation had minimal effect on the Nusselt number.

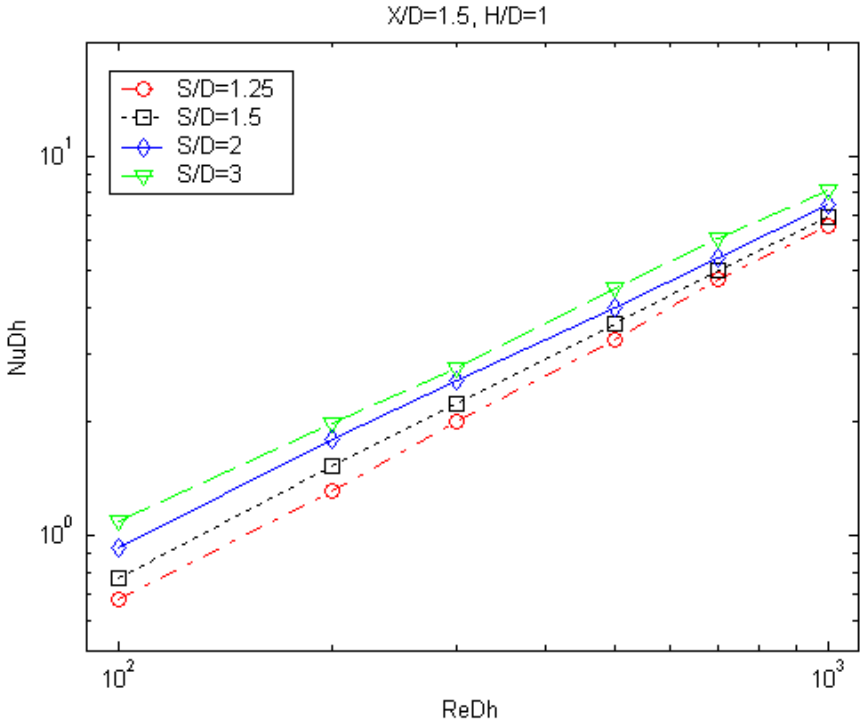

Figure 20 Effect Reynolds number on Nusselt number

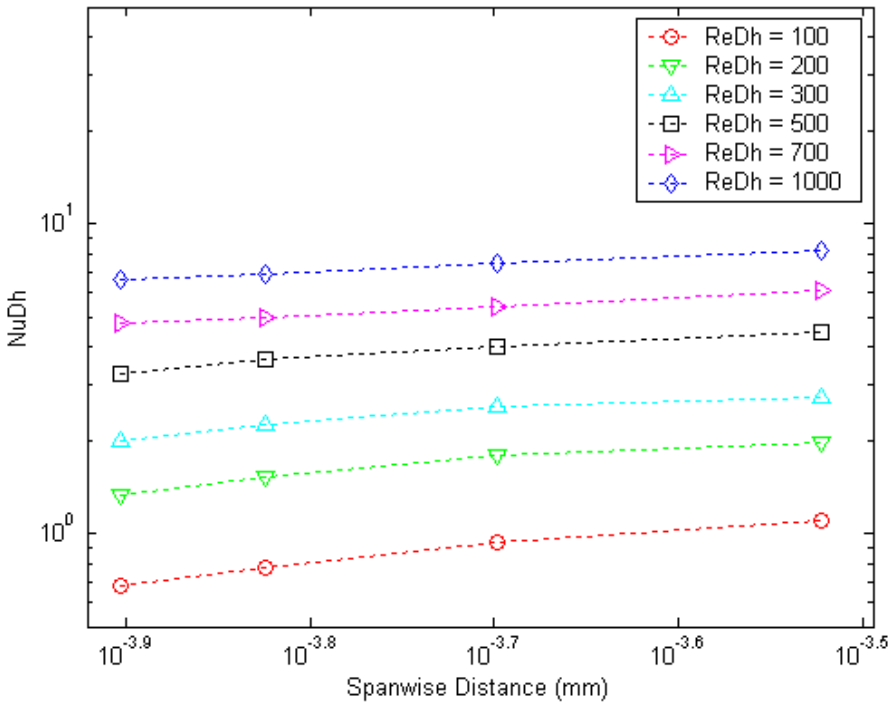

Figure 21 Effect of spanwise distance on Nusselt number

b. Effects of Friction Factor

The friction factor results have also been plotted for each configuration in a similar manner to *X/D*. The graph in Figure 22 shows friction factor plotted against Reynolds number on a logarithmic scale for specific *S/D* configurations. The dimensionless friction factor is based upon the hydraulic diameter and has a direct correlation with the flow velocity. Therefore, an increase in the *S/D* ratio will result in greater hydraulic diameter causing a decrease in the inlet velocity to maintain a specific Reynolds number. Figure 22 clearly demonstrates that the friction factor increases with decreasing Reynolds number.

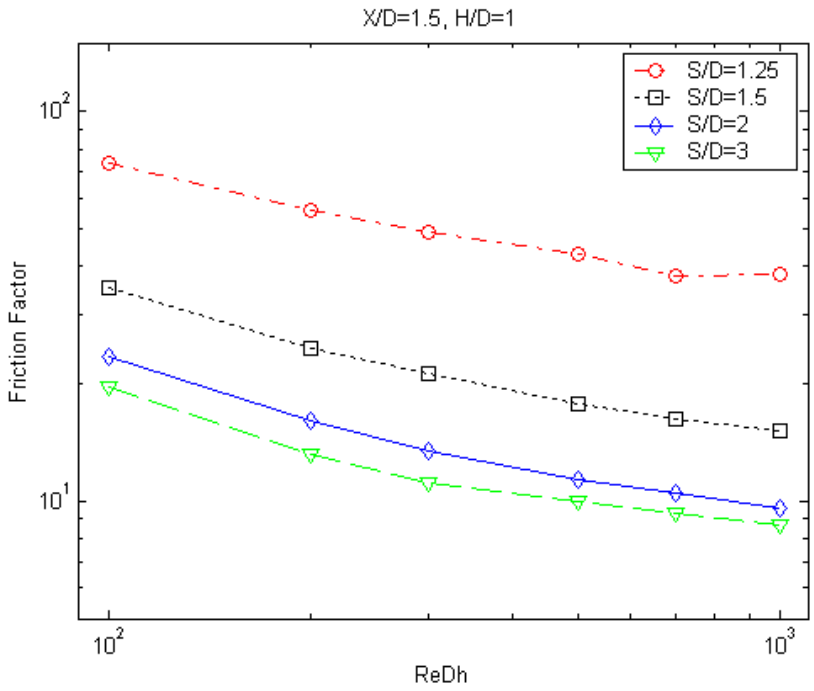

Figure 22 Effect of Reynolds number on friction factor

It can be seen from Figure 23 that the friction factor varied significantly with changes in *S/D*. All the configurations have similar characteristics and trends showing that the friction factor reduces with increasing *S/D*. When *S/D* is reduced, the smaller spanwise spacing causes the entrance flow passage area to shrink. Therefore, the flow enters at a higher velocity and is forced to follow a tortuous path through the pin-fin array section. This causes a large resistance to the flow and causes large pressure drops to occur. On the contrary, increasing the *S/D* ratio will open up the flow passages and the flow is allowed to pass more smoothly through the array section with relatively less resistance. This explains the lower friction factor that was observed for higher *S/D*.

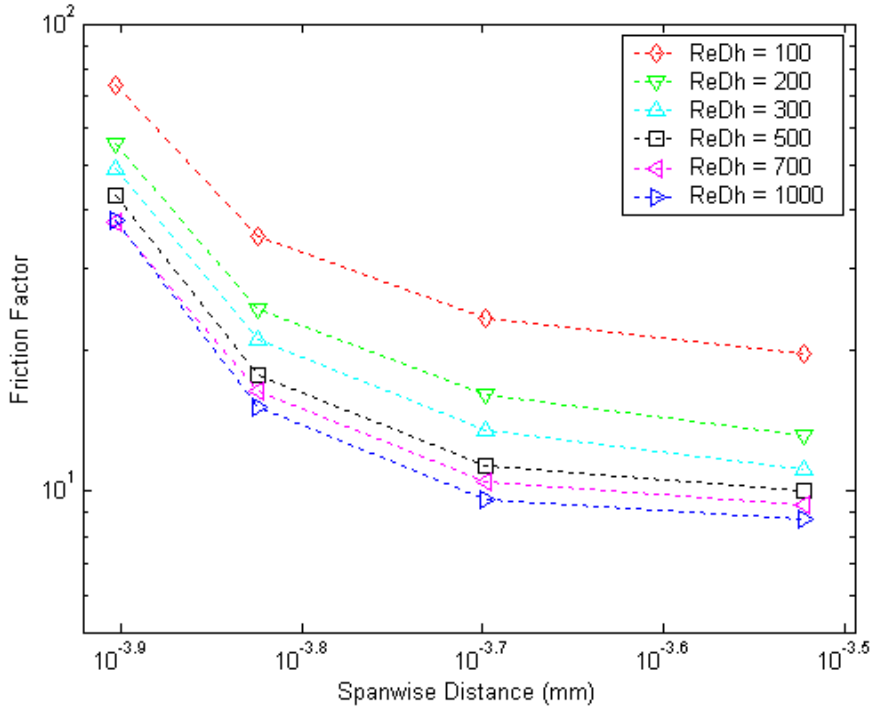

Figure 23 Effect of spanwise distance on friction factor

Figure 24 shows two numerical solutions of the flow through the extreme cases of *S/D*=3 and *S/D*=1.25 to further illustrate the effect of velocity with varying *S/D*. It can be seen from the Figure 24 that the flow for the lower *S/D* has to negotiate a serpentine path through the pin-fins array whereas for the higher *S/D*, the flow is able to pass smoothly through the array without much resistance. It was observed that the fluid flow at larger *S/D* has minimal interaction with the pin surfaces. This phenomenon contributes greatly to the reduction of pressure drop.

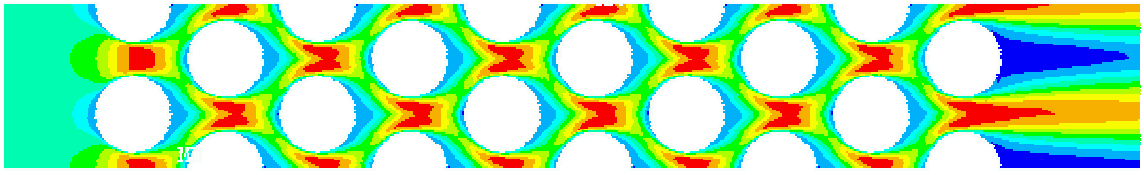

Re_{Dh}=100, *S/D*=1.25, *X/D*=1.5, *H/D*=1

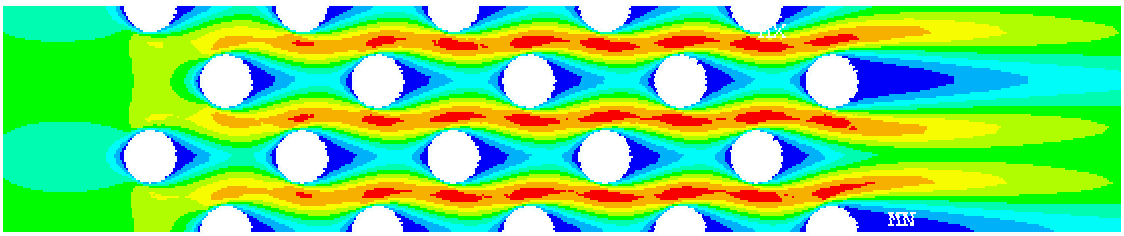

Re_{Dh}=100, *S/D*=3, *X/D*=1.5, *H/D*=1

Figure 24 Contour plots for flow through array

c. Heat Transfer Coefficient

The effect of Reynolds number on the heat transfer coefficient is illustrated in Figure 25 for *S/D*=3. It can be observed that the Reynolds number has a great effect on the heat transfer coefficient as in the case of *X/D*. As discussed in the preceding section, the greater flow velocity will contribute to significant increases in heat transfer coefficient. It appears that the effect of *S/D* variation is minimal for lower Reynolds number, and becomes more noticeable at larger Reynolds numbers. This effect can be seen in the contour plot for the extreme cases of Reynolds number on the heat transfer rate. The lighter shade represents a higher heat transfer rate.

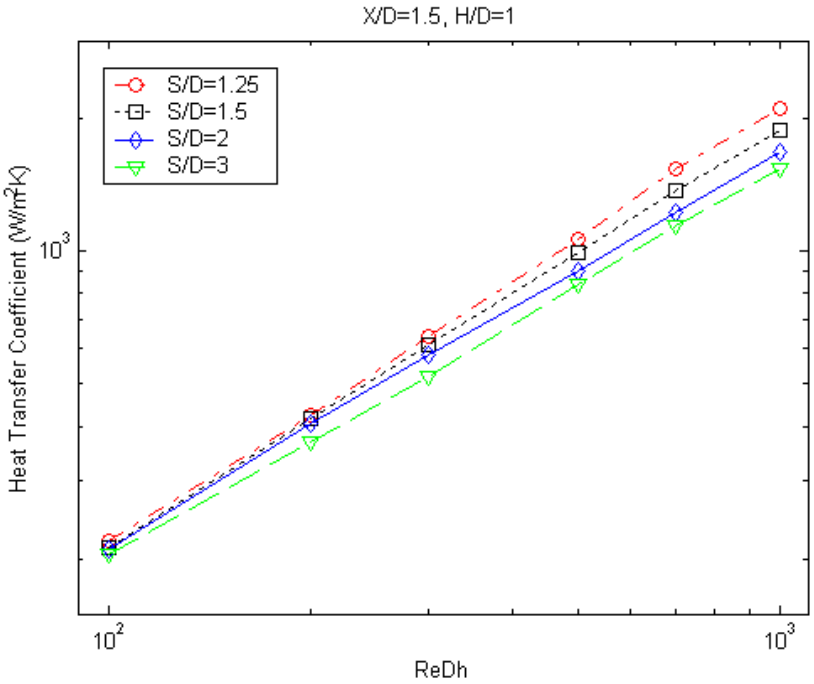

Figure 25 Effect of Reynolds number on heat transfer coefficient

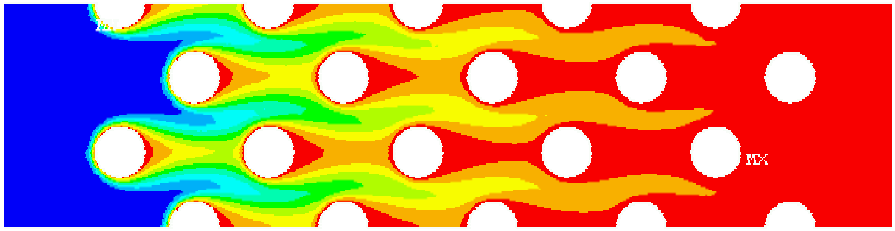

Re=100, *X/D*=1.5, *S/D*=3.0

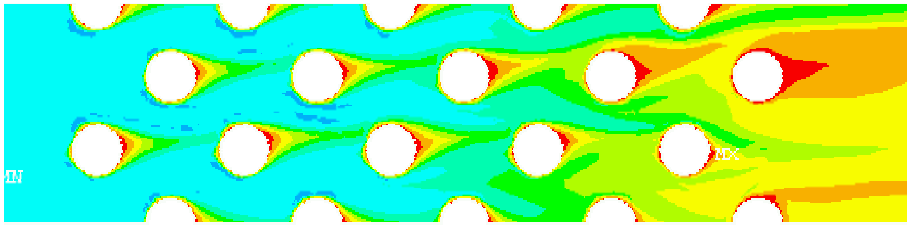

Re=1000, *X/D*=1.5, *S/D*=3.0

Figure 26 Contour plots of heat transfer rate on various Reynolds number

It is apparent from Figure 27 that the effect of *S/D* variation has minimal effect on the heat transfer coefficient. Although the heat transfer rate was noticed to increase with amplifying *S/D* ratio, it does not correspond to the increase in heat transfer coefficient. It was observed that the rate of increase of the wetted area due to increasing *S/D* was greater then the rate of increase for the heat transfer rate. This resulted in the decrease of heat transfer coefficient with increasing *S/D*. Figure 28 contains contour plots showing the effect of heat transfer rate on varying *S/D*. As before, the higher heat transfer rate is represented by the lighter shade.

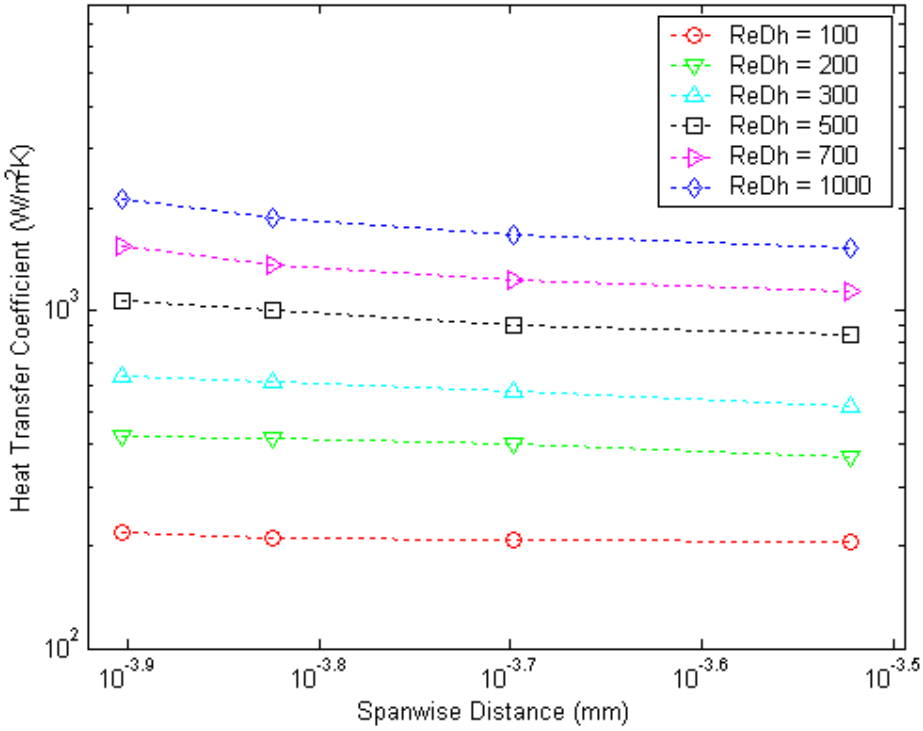

Figure 27 Effect of spanwise distance on heat transfer coefficient

Re=100, *X/D*=1.5, *S/D*=1.25

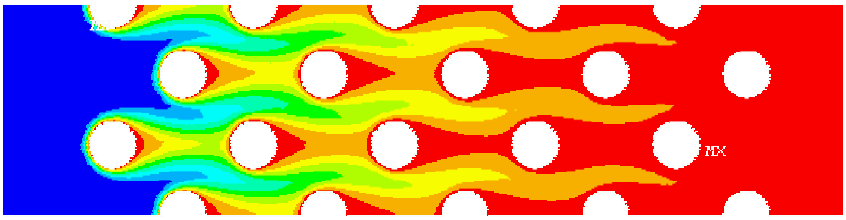

Re=100, *X/D*=1.5, *S/D*=3.0

Figure 28 Contour plots of heat transfer rate for *S/D*

d. Performance Comparisons

The heat transfer coefficient is plotted against the friction power in Figure 29 to investigate the optimal design configuration that would maximize the heat transfer

rate while minimizing frictional losses in the flow. A careful analysis revealed that the most efficient configuration for constant *X/D*=1.5 and *H/D*=1 was observed to be for *S/D*=3, and the least favorable was for *S/D*=1.25. It was noticed that the more desirable case of *S/D*=3 used a much lower friction power then *S/D=1.25* to achieve the same heat transfer coefficient. For example, in the case of Re_{Dh} ranging from100 to 200, *S/D*=3 only required 5 W/m^2 as compared to *S/D*=1.25 using 380 W/m^2 to increase the heat transfer coefficient from 200 W/m^{2}K to 370 W/m^{2}K. For *S/D*=1.25, especially towards the higher range of Reynolds numbers, shows that a lower Reynolds number is required to achieve the same heat transfer coefficient as *S/D*=3. This benefit is however overwhelmed by the need for much greater friction power.

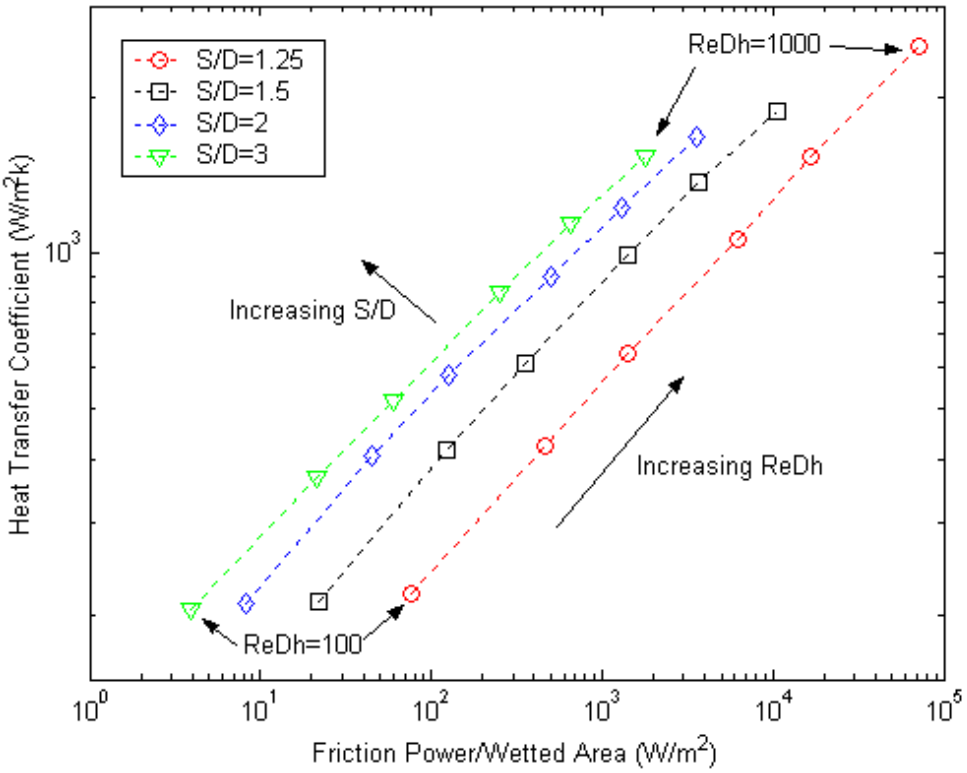

Figure 29 Effect of spanwise distance on performance

THIS PAGE INTENTIONALLY LEFT BLANK

C. EFFECTS OF PIN HEIGHT RATIO

This section will discuss the effect of pin height ratio variation on the heat exchanger performance. Numerical simulations were performed on various configurations and the findings are described in the following sections.

1. Test Approach

Based on the deductions obtained from the preceding sections, a fixed axial pitch and spanwise spacing were used for the numerical model. The ratios used were *S/D* =1.5, *S/D* =3, and *H/D* varying from 1 to 3. The Reynolds numbers were varied from 100 to 1000.

2. Results and Discussion

a. Effects of Pin Height Ratio on Nusselt Number

Figure 30 shows Nusselt number plotted against Reynolds number for various *H/D* configurations. It was observed that all the configurations followed a similar trend with Nusselt number increasing with Reynolds number. Magnification of *H/D* causes the hydraulic diameter to increase resulting in lower flow velocities for a given Reynolds number, thus also resulting in lower heat transfer coefficients. Since the heat transfer coefficient decrease is insignificant compared to the increase in hydraulic diameter, the Nusselt number increases proportionally with Reynolds number. These deductions are further illustrated in Figure 31 showing increasing Nusselt number with pin height.

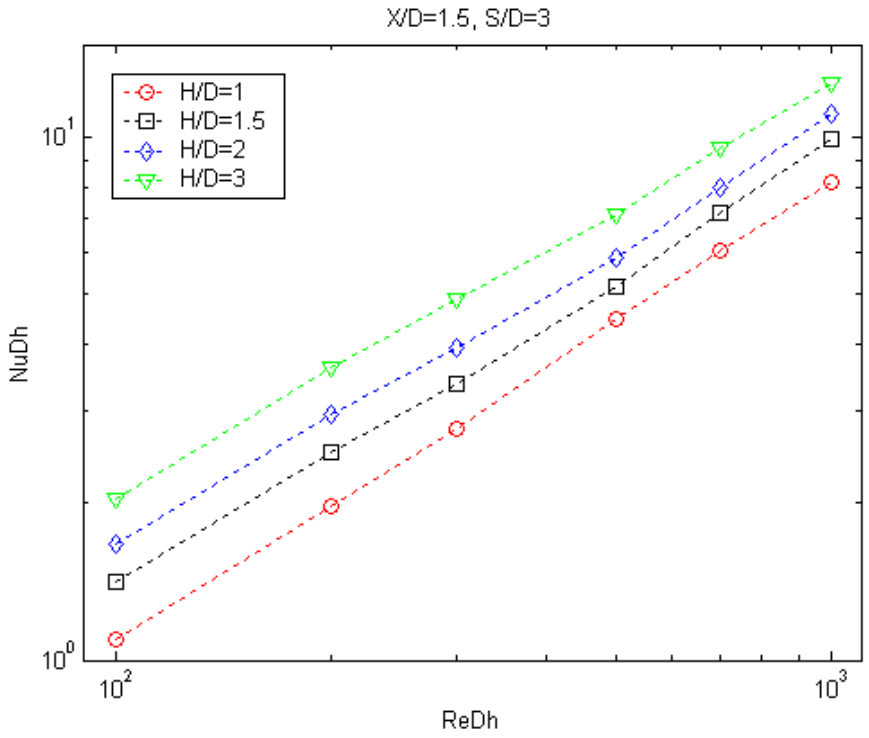

Figure 30 Effect of Reynolds number on Nusselt number

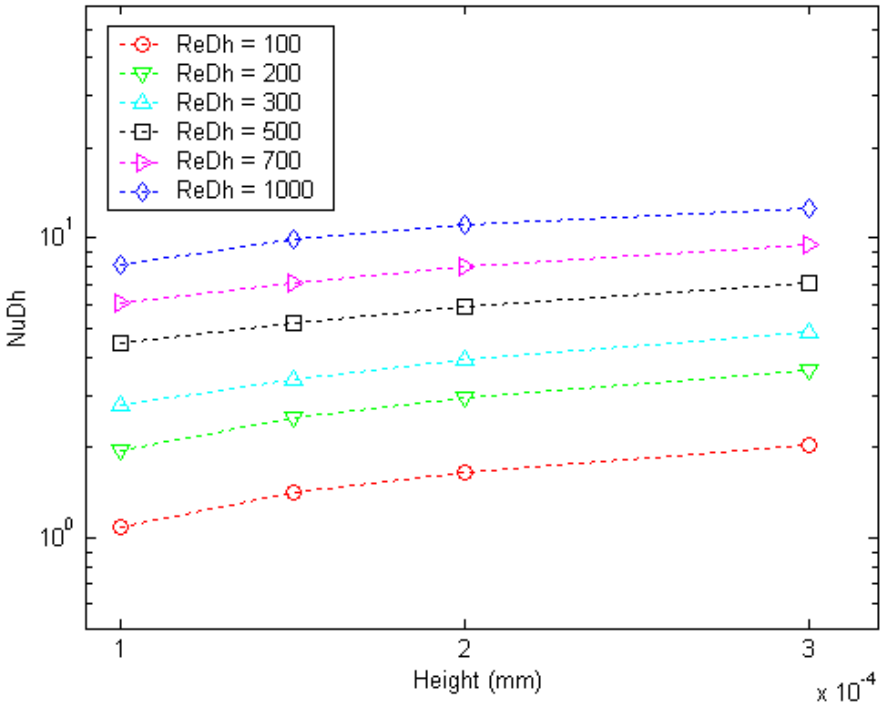

Figure 31 Effect of pin height on Nusselt number

b. Effect of Pin Height Ratio on Friction Factor

Figure 32 shows friction factor plotted against Reynolds number for all *H/D* configurations. The figure shows that the friction factor increases with reducing Reynolds number. It was observed that reducing the *H/D* causes lower flow velocities and smaller pressure drops for a specific Reynolds number. The friction factor is relative to the hydraulic diameter, pressure drop and the inverse of velocity. It was noticed that the decrease in pressure drop was insignificant as compared to rate of decrease in the square of velocity. This resulted in the increase in friction factor with increasing *H/D* ratio although it was noticed that the pressure loss for larger *H/D* was dramatically lower than for smaller *H/D* configurations. This deduction is further illustrated by plotting the friction factor against the pin height as shown in Figure 33.

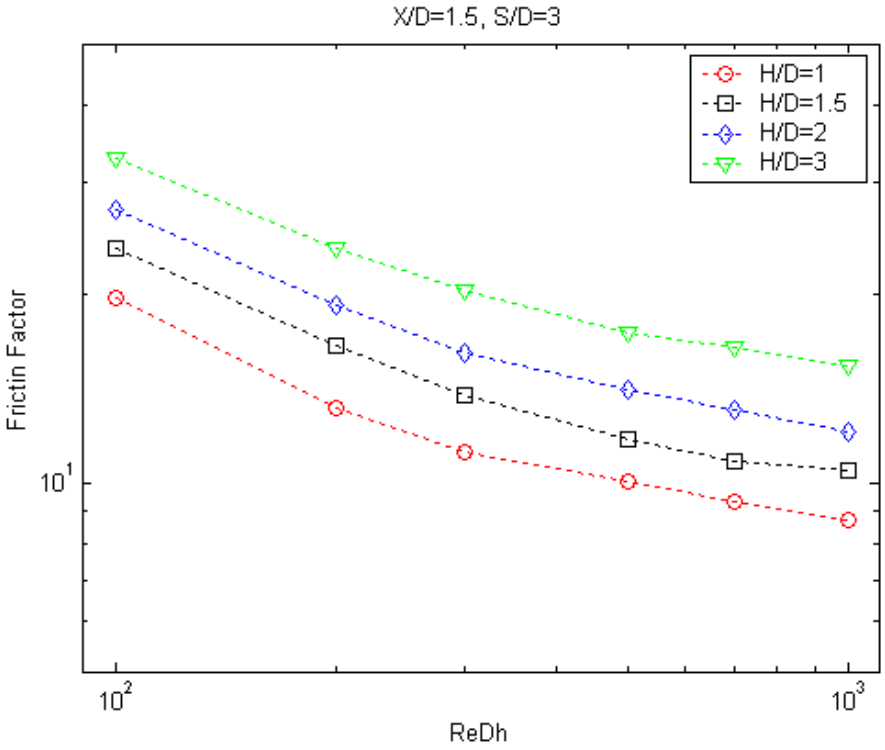

Figure 32 Effects of Reynolds number on friction factor

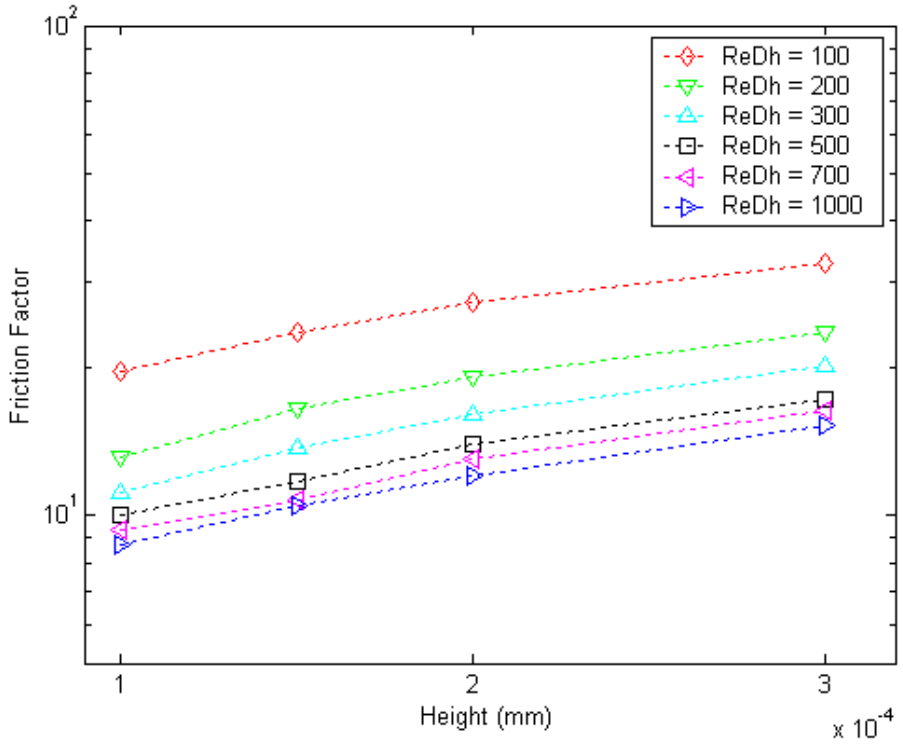

Figure 33 Effects of pin height on friction factor

c. Effect of Pin Height Ratio on Heat Transfer Coefficient

The effect of Reynolds number on the heat transfer coefficient can be seen in Figure 34. It is apparent that the effect of *H/D* variation is insignificant for lower Reynolds numbers, and the effect of *H/D* becomes more significant with increasing Reynolds number. The effect of pin height on heat transfer coefficient is shown in Figure 35. It was observed that the variation in pin height has minimal effect on the heat transfer coefficient.

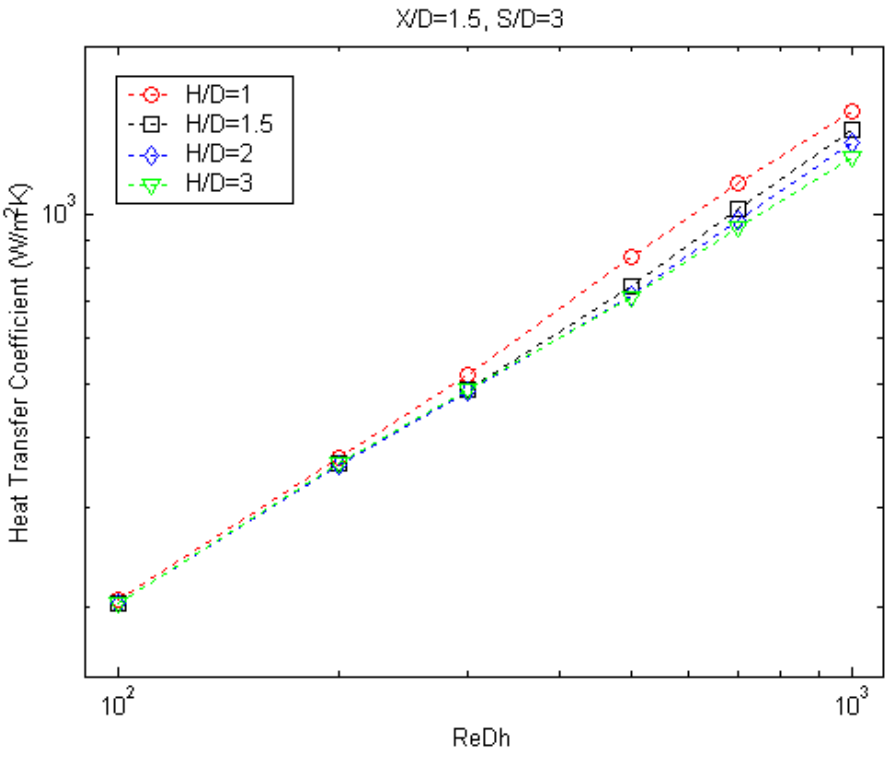

Figure 34 Effect of Reynolds number on heat transfer coefficient

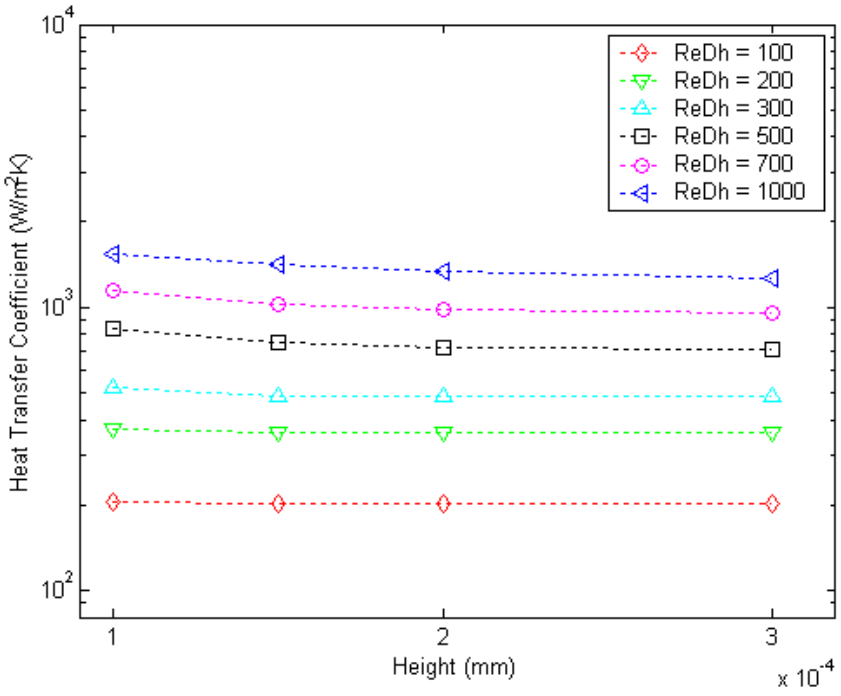

Figure 35 Effect of pin height on heat transfer coefficient

Figure 36 shows that the increase in pin height ratio will reduce the area density. The area density is plotted against the heat transfer coefficient as shown in Figure 37. It was noticed that the increase in area density has no significant effect on the heat transfer coefficient.

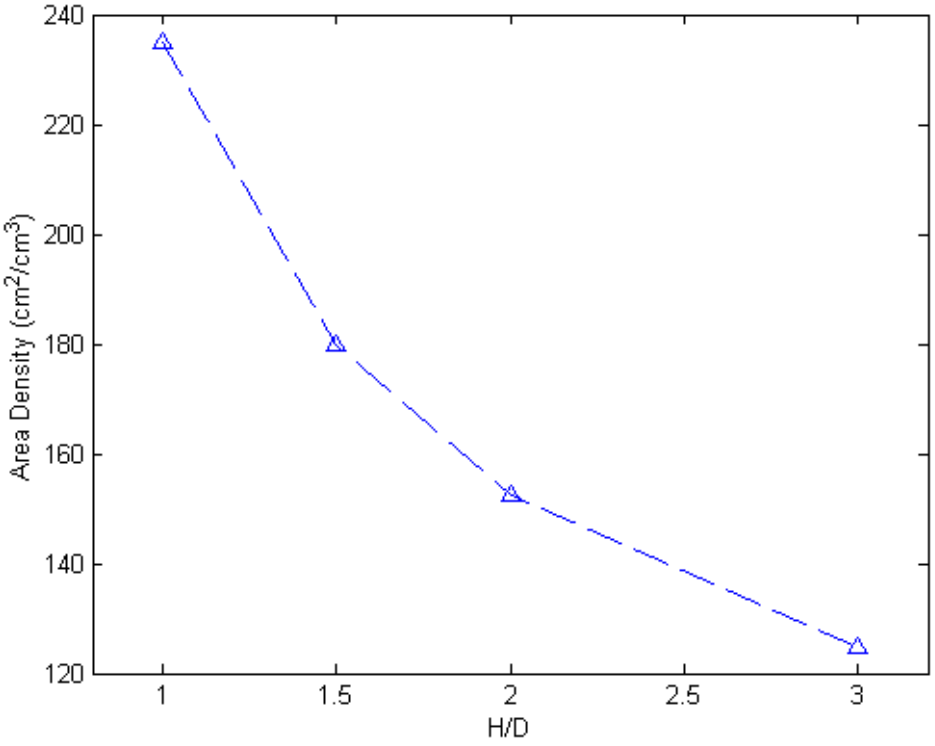

Figure 36 Effect of H/D on area density

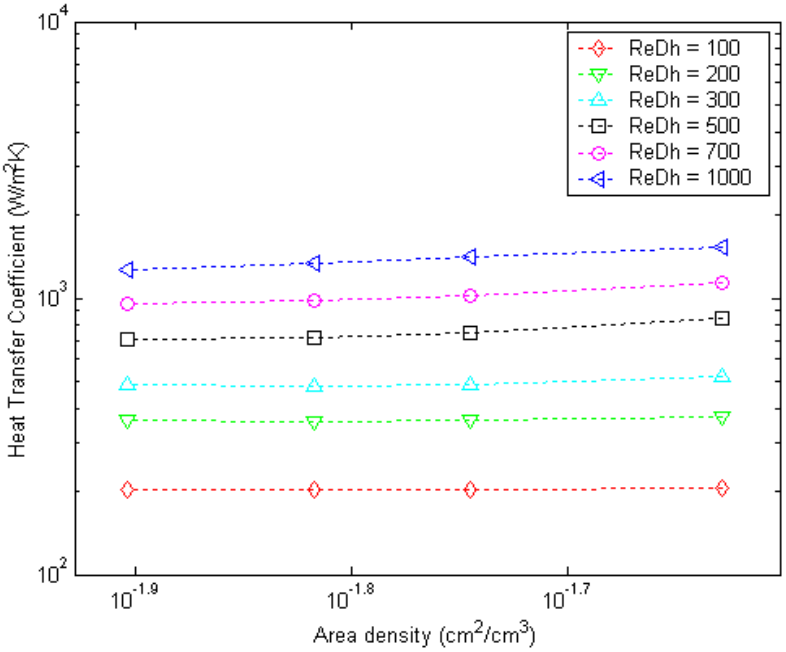

Figure 37 Effect of area density on heat transfer coefficient

Figure 38 shows that the larger pin height ratios result in greater heat transfer rates. The lighter shades represent higher heat transfer rates. This is due to the greater pin surface available for interaction with the airflow as it swirls around the longer pins.

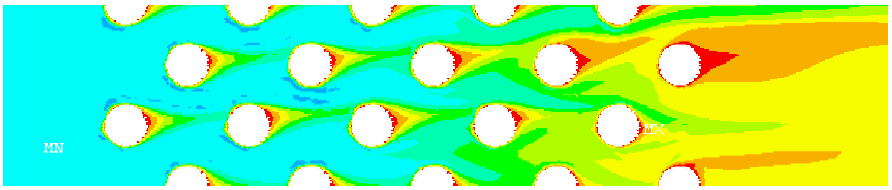

Re=100, *X/D*=1.5, *S/D*=3.0, *H/D*=1.0

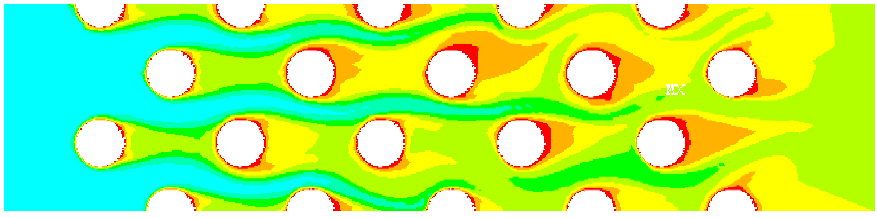

Re=1000, *X/D*=1.5, *S/D*=3.0, *H/D*=3.0

Figure 38 Contour plots of heat transfer coefficient for *H/D*

d. Effects of Local Heat Transfer Coefficient at the Pin Surface

The local heat transfer coefficient at the pin surface can be evaluated by plotting the data obtained from the numerical simulation. This section will discuss the results obtained from the numerical solution for the configuration $X/D=S/D=2.0$ at $Re_{Dh}=500$. Figure 39 shows a 3-D contour plot of this configuration with the flow from left to right.

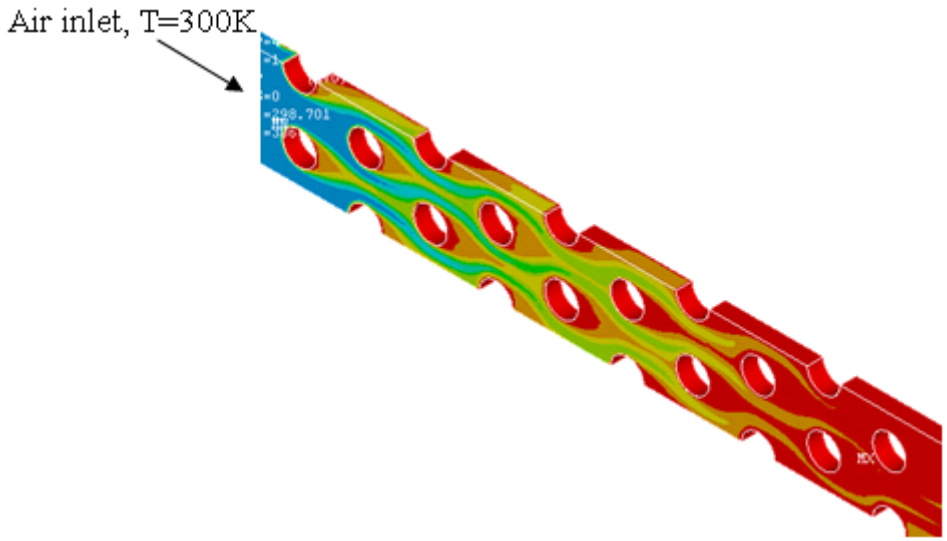

Figure 39 3D plot of heat transfer coefficient

The local heat transfer coefficient at the pin surfaces can be observed using a radial plots as shown in Figure 40. The plots illustrate the angular variation of the heat transfer coefficient on the surface of pins from various rows. The results were taken circumferentially at two locations along the height (H) of the pin, at z=H/3 and z=3H/4 from the endwall.

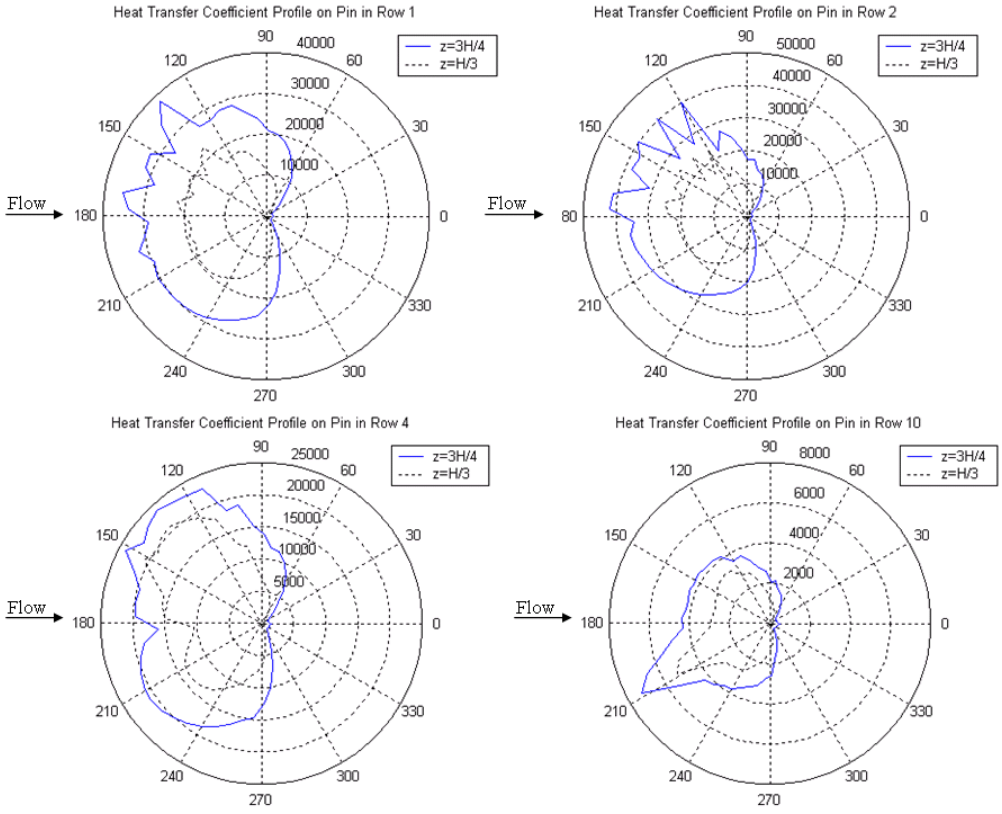

Figure 40 Radial plots of heat transfer coefficient

The flow is from left to right and the plots shows that the local heat transfer coefficient is highest on the leading face of the pin between 90 to 270 degrees. The heat transfer coefficient reduces significantly on the trailing face of the pin. This is due to the separation of the flow from the surface of the pins. From this figure it appears that the heat transfer coefficient is lower on the pin surface nearer the endwall, at z=H/3 because of boundary layer effects from the endwall.

The general trend is an initial rise in the local heat transfer coefficient among the first three to five rows followed by a subsequent gradual decline. It was observed from Figure 40 that the highest local heat transfer coefficient occurred at about row 2.

e. Performance Comparisons

The heat exchanger performance can be determined by plotting the heat transfer coefficient against the friction power as shown in Figure 41. As in the preceding sections, the benefit of varying the *H/D* ratio can be evaluated to determine the optimal design configuration to maximize the heat transfer rate without incurring high frictional losses in the flow

The amount of increase in friction power needed to increase the heat transfer coefficient was examined using Figure 41. It was observed for the case of Re_{Dh} ranging from100 to 200, *H/D*=3 required 5 W/m^2 whereas *H/D*=1 needed 7 W/m^2 to increase the heat transfer coefficient from 200 W/m^{2}K to 360 W/m^{2}K. The difference in friction power needed was noticed to be small. Therefore, it was apparent that both configurations are comparable in term of the amount of friction power required to raise the Re_{Dh}.

Although *H/D*=1 needed slightly lower Reynolds number to achieve a similar heat transfer coefficient as *H/D*=3, the friction power required was much greater. It can be seen that the friction power required by *H/D*=1 to reach a specific heat transfer coefficient of 1200 W/m^{2}K was 900 W/m^2 as compared to 470 W/m^2 for *H/D*=3.

Coupled with the earlier finding that the variation in H/D has minimal effect on heat transfer coefficient, it is apparent that for constant *X/D*=1.5 and *S/D*=3, the case of *H/D*=3 shows better performance than *H/D*=1.

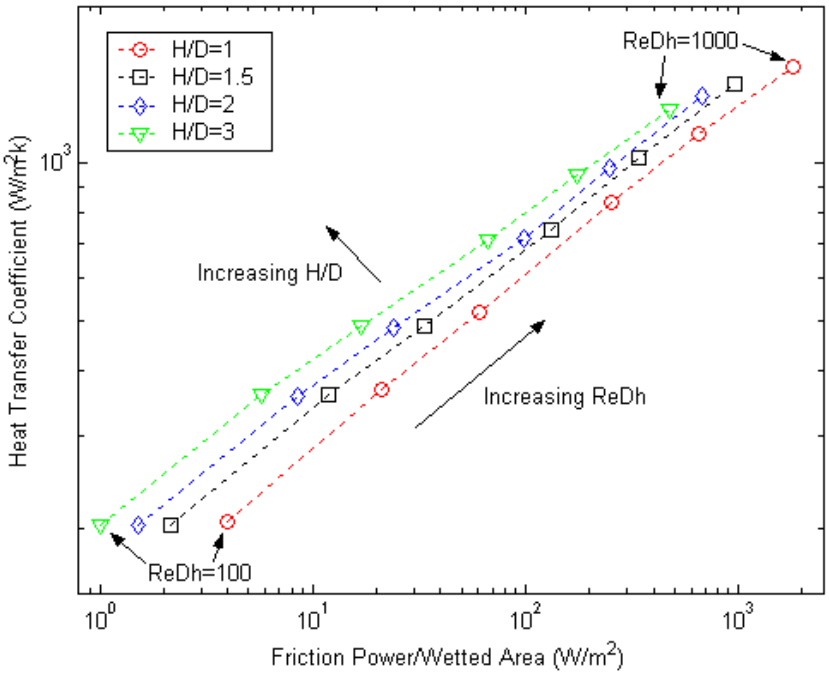

Figure 41 Effect of *H/D* on performance

THIS PAGE INTENTIONALLY LEFT BLANK

IV. CONCLUSIONS

The primary objectives of this study were successfully met by the numerical simulation of a pin-fin heat exchanger for varying configurations and Reynolds numbers. The results were analyzed to determine an optimal configuration that would maximize the performance of a micro heat exchanger.

Due to the fact that micro devices have a large surface to volume ratio, factors related to surface effects have a greater impact on the flow and heat transfer at small scales. Therefore, it is crucial to investigate the thermo-fluid characteristics of laminar flow in the low Reynolds number range.

Variations in axial pitch were shown to have no appreciable effect on Nusselt number and friction factor. However, reductions in axial pitch can produce a significant increase in heat exchanger performance based on pressure drop costs. These results were important for determining the optimal configuration for *X/D*. It was found that reducing axial pitch is more cost effective than increasing Reynolds number to enhance the performance of the micro heat exchanger.

The small hydraulic dimensions of micro flow passages present a large frictional pressure drop in the pin-fins array. In order to keep the pressure drop within limits, the *S/D* ratio should be amplified to minimize frictional losses in the flow. It was demonstrated that variation in spanwise distance had minimal effect on the Nusselt Number and heat transfer coefficient but has a great effect on the friction frictional losses. It was shown that amplifying the spanwise distance reduces the friction power significantly.

Variations in *H/D* had significant effects on heat exchanger performance. It was apparent that the variation in pin height has no significant effect on the heat transfer coefficient. It was found that higher *H/D* ratio requires lower friction power to achieve the same heat transfer coefficient as lower *H/D*. It was found that the local heat transfer coefficients were highest among the first three to five rows and the maximum local heat transfer coefficient occurred at row 2.

By combining all the results obtained from the report, it has been deduced from the current numerical simulations that the optimum theoretical configuration lies in the vicinity of a configuration with X/D=1.25, S/D = 3.0 and H/D = 3.0, and with a pin diameter D=100 μm.

APPENDIX A. SAMPLE ANSYS MACRO

The macro was used to input into ANSYS to facilitate the generation of the numerical solutions. The method was efficient and systematic as a large number of numerical models were required for this study.

A template macro was created and different parameters such as Reynolds number, pin spacing and height ratio, axial pitch, inlet air and wall temperature, reference pressure and mesh density were used for each configuration.

These variables were automatically constructed and meshed the desired model and set ANSYS solution parameters to include solver type and iteration number. The computational analysis was then performed and solution results were obtained. The following shows a sample of the macro.

SAMPLE MACRO

```
/TITLE,RUN #2, RE=100,X/D=1.25,S/D=1.5,H/D=1, TW =306,H/V/P
=7/12/2,10ATM,5INF
! CREATES AN ENDLESS 1.5 PIN FIN ARRAY WITH 10 ROWS
! UNHEATED ENTRY AND EXIT REGIONS
!*****************************************

!************************
!*       INPUT VARIABLES *
!************************

!ENTER YOUR REYNOLD'S NUMBER (VANFOSSEN DEFINITION)
REDH =100

!PIN DIAMETER [M]
D = 0.0001

!ENTER YOUR X/D (CYLINDER SPACING IN THE FLOW DIRECTION)
XD = 1.25

!ENTER YOUR S/D (SPANWISE SPACING NORMAL TO FLOW)
SD = 1.5

!ENTER YOUR H/D (PIN HEIGHT/DIAMETER RATIO)
HD = 1.0
```

```
!***** MASHING PARAMETERS *****

!ENTER XY (H)/AND Z (V) GRID SCALING
H = 7.4
V = 12
!ENTER PIN FACTOR
P = 2


!INLET TEMPERATURE
TIN = 300

!WALL TEMPERATURE
TWALL = 306

!AMBIENT TEMPERATURE
TATM = 273.15

TFILM = (TWALL+TIN)/2

!ENTER REFERENCE PRESSURE IN PA
PREF = 1013500

!CALCULATE KINEMATIC VISCOSITY USING SUTHERLAND LAW
RHO = PREF/(287*TFILM)
RHO300 = PREF/(287*TIN)

!FINDING COEFF OF VISCOSITY USING SUTHERLAND LAW
!SUTHERLAND LAW CONSTANTS ARE
!SAIR FOR AIR IS 110.4 [DEGREE K]
SAIR = 110.4
MUO = 1.71E-005
MU = (TATM+SAIR)/(TFILM+SAIR)*MUO*(TFILM/TATM)**(3/2)

!KINEMATIC VISCOSITY
NU = MU/RHO


!*********************************************
!*       TEST SECTION CONFIGURATION CALCULATION     *
!*********************************************

!AXIAL PITCH / PIN CENTER TO PIN CENTER STREAMWISE DISTANCE
DDX = XD*D
```

```
!PIN CENTER TO PIN CENTER SPANWISE DISTANCE
SSY = SD*D

! PIN HEIGHT OR DEPTH
HT = HD*D

!CALCULATED FOR A UNIT CELL, I.E. UC (S*2X)
!VARRAY,UC
VARRAY = 2*SSY*DDX*HT

!VPIN,UC
VPIN = 3.14159*HT*(D**2)/4

!VOPEN,UC
VOPEN = VARRAY - 2*VPIN
AWPIN = 3.14159*D*HT
! AFEET IS THE PIN ROUND END SURFACE
AFEET = 3.14159*(D**2)/4
! AWALL IS THE SURFACE AREA OF BOTH SIDE WALLS
AWALL = 2*SSY*DDX - 2*AFEET
! AW IS THE WETTED AREA INCLUDING THE PIN SURFACE AREAS
AW = 2*AWPIN + 2*AWALL

ABAR = VOPEN/(2*DDX)
ADUCT = SSY*HT
DPRIME = 4*VOPEN/AW



!**********************************
!*       INLET VELOCITY CALCULATION        *
!**********************************


VIN = REDH*MU*ABAR/(DPRIME*RHO300*ADUCT)


!*********************************************
!*       CALCULATE ENTRY LENGTH FOR LAMINAR FLOW*
!*********************************************

ENTRYDH = 2*HT
ENTRYRE = VIN*ENTRYDH/NU
ENTRY = 0.06*ENTRYDH*ENTRYRE
ENTRYINIT = ENTRY
```

```
!ENTER EXIT LENGTH
EXIT = ENTRY/2

!TOTAL LENGTH OF PIN SECTION WITH (XD/2)*D BEFORE THE
!LEADING EDGE AND (XD/2)*D FOLLOWING THE TRAILING EDGE
!OF THE LAST ROW OF PINS.
XLENGTH= (DDX*10)

!TOTAL WIDTH OF ANSYS MODEL, INSULATED WALL TO SYM PLANE.
YLENGTH= (SSY*1.5)

!*****************************************
!*       THIS MODULES SETS FLOTRAN PARMS         *
!*****************************************

!****** SELECTS OPERATING PREFERENCE *******
/NOPR
/PMETH,OFF,0
KEYW,PR_SET,1
KEYW,PR_STRUC,0
KEYW,PR_THERM,1
KEYW,PR_FLUID,0
KEYW,PR_ELMAG,0
KEYW,MAGNOD,0
KEYW,MAGEDG,0
KEYW,MAGHFE,0
KEYW,MAGELC,0
KEYW,PR_MULTI,1
KEYW,PR_CFD,1
/GO
!*
/COM,
/COM,PREFERENCES FOR GUI FILTERING HAVE BEEN SET TO DISPLAY:
/COM,  THERMAL
/COM,  FLOTRAN CFD
!*
/UNITS,SI
/PREP7
!*
!SELECTS ELEMENT TYPE
ET,1,FLUID142
!*
!*****************INITIAL SOLN OPTIONS*************
FLDATA1,SOLU,TRAN,0
FLDATA1,SOLU,FLOW,1
FLDATA1,SOLU,TEMP,0
```

```
FLDATA1,SOLU,TURB,0
FLDATA1,SOLU,COMP,0
FLDATA1,SOLU,VOF,0
FLDATA1,SOLU,SFTS,0
FLDATA1,SOLU,IVSH,0
FLDATA1,SOLU,SWRL,0
FLDATA1,SOLU,SPEC,0
FLDATA1,SOLU,ALE,0
!*****************INITIAL EXECUTION CONTROL********
/COM,,STEADY STATE ANALYSIS,0
FLDATA2,ITER,EXEC,30,
FLDATA2,ITER,OVER,0,
FLDATA2,ITER,APPE,0,
FLDATA3,TERM,VX,0.01,
FLDATA3,TERM,VY,0.01,
FLDATA3,TERM,VZ,0.01,
FLDATA3,TERM,PRES,1E-008,
FLDATA3,TERM,TEMP,1E-008,
FLDATA3,TERM,ENKE,0.01,
FLDATA3,TERM,ENDS,0.01,
FLDATA5,OUTP,SUMF,10,
FLDATA5,OUTP,YPLU,T
!*****************ADDED TO MAKE DENSITY AN OUTPUT
FLDATA5,OUTP,DENS,T,
!*
/PREP7
FINISH
/PREP7
!************INITIAL FLUID PROPERTIES (CONSTANT
DENSITY)*************
FLDATA12,PROP,DENS,4
FLDATA13,VARY,DENS,0
FLDATA12,PROP,VISC,4
FLDATA13,VARY,VISC,1
FLDATA12,PROP,COND,4
FLDATA13,VARY,COND,1
FLDATA12,PROP,SPHT,4
FLDATA13,VARY,SPHT,1
!*
FLDATA7,PROT,DENS,AIR-SI
FLDATA8,NOMI,DENS,-1
FLDATA9,COF1,DENS,0
FLDATA10,COF2,DENS,0
FLDATA11,COF3,DENS,0
FLDATA7,PROT,VISC,AIR-SI
FLDATA8,NOMI,VISC,-1
```

```
FLDATA9,COF1,VISC,0
FLDATA10,COF2,VISC,0
FLDATA11,COF3,VISC,0
FLDATA12,PROP,IVIS
FLDATA7,PROT,COND,AIR-SI
FLDATA8,NOMI,COND,-1
FLDATA9,COF1,COND,0
FLDATA10,COF2,COND,0
FLDATA11,COF3,COND,0
FLDATA7,PROT,SPHT,AIR-SI
FLDATA8,NOMI,SPHT,-1
FLDATA9,COF1,SPHT,0
FLDATA10,COF2,SPHT,0
FLDATA11,COF3,SPHT,0
!*
!***SELECT REF TEMP = 300K**********
FLDATA14,TEMP,NOMI,300
FLDATA14,TEMP,TTOT,300
FLDATA14,TEMP,BULK,300
FLDATA15,PRES,REFE,PREF
!*
!***********CHANGE PRES CFD SOLVER TO PBCGM**********
FLDATA18,METH,PRES,6
FLDATA22,MAXI,PRES,1000,
FLDATA20,SRCH,PRES,2,
FLDATA20B,PBCG,FILL,6,
FLDATA21,CONV,PRES,1E-012,
!FLDATA25,RELX,PRES,0.2,
!*
!************TEMP CFD SOLVER IS PGMR******************
FLDATA18,METH,TEMP,4,
FLDATA22,MAXI,TEMP,1000,
FLDATA20,SRCH,TEMP,12,
FLDATA20A,PGMR,FILL,6,
FLDATA20A,PGMR,MODP,0,
FLDATA21,CONV,TEMP,1E-12,
FLDATA23,DELT,TEMP,1E-010,
!*
FLDATA34,MIR,MOME,0.5,
FLDATA34,MIR,TEMP,0.5,
!*FLDATA31,CAPP,TEMP,T,
!*************************************
!THE MODIFIED INERTIAL RELAXATION VALUE SHOULD BE BETWEEN 0.1
AND 1.0.
!A LARGER VALUE LEADS TO MORE RELAXATION.
```

```
!TO ACHIEVE A FASTER CONVERGENCE RATE, USE THE SMALLEST VALUE
POSSIBLE.
!*
!**********ADVECTION PARMS**************
FLDATA,ADVM,MOME,MSU
FLDATA,ADVM,TURB,MSU
FLDATA,ADVM,PRES,MSU
FLDATA,ADVM,TEMP,MSU
!*


!***********************
!*       BLOCK & PINS       *
!***********************

/PREP7
!CREATES INITIAL BLOCK WITH EXTRA LENGTH

!START IN MIDDLE OF FIRST ROW
XLOC=ENTRY + DDX/2
START=ENTRY

*DO,I,1,5
BLOCK,ENTRY,ENTRY+DDX,0,YLENGTH,0,HT/2

CYL4,XLOC,SSY/2,D/2,,,,HT/2
CYL4,XLOC,(SSY*1.5),D/2,,,,HT/2
BLOCK,ENTRY+DDX,ENTRY+2*DDX,0,YLENGTH,0,HT/2
CYL4,(XLOC+DDX),0,D/2,,,,HT/2
CYL4,(XLOC+DDX),SSY,D/2,,,,HT/2
XLOC=XLOC + (DDX*2)
ENTRY=ENTRY + (DDX*2)
*ENDDO

!***************SUBTRACT PINS*******************
FLST,2,10,6,ORDE,10
!FLST,2=FIRST COMMAND ARGUMENT,# OF ITEMS PICKED,TYPE OF ITEMS
PICKED 6=VOLUME #,ORDER=DATA IN ORDERED LIST, # OF NUMBER OF
ITEMS)
!SELECTING THE VOLUMES TO BE SUBTRACTED FROM, FIRST COMMAND
ARGUMENT FOR VSBV
FITEM,2,1
FITEM,2,4
FITEM,2,7
FITEM,2,10
FITEM,2,13
```

```
FITEM,2,16
FITEM,2,19
FITEM,2,22
FITEM,2,25
FITEM,2,28
FLST,3,20,6,ORDE,20
!SELECTING THE PINS TO BE SUBTRACTED FROM, SECOND COMMAND ARGUMENT FOR VSBV
FITEM,3,2
FITEM,3,-3
FITEM,3,5
FITEM,3,-6
FITEM,3,8
FITEM,3,-9
FITEM,3,11
FITEM,3,-12
FITEM,3,14
FITEM,3,-15
FITEM,3,17
FITEM,3,-18
FITEM,3,20
FITEM,3,-21
FITEM,3,23
FITEM,3,-24
FITEM,3,26
FITEM,3,-27
FITEM,3,29
FITEM,3,-30
VSBV,P51X,P51X
!************ADD ENTRY BLOCK******************
BLOCK,0,START,0,YLENGTH,0,HT/2
!************ADD EXIT BLOCK*******************
BLOCK,START+XLENGTH,START +XLENGTH+EXIT,0,YLENGTH,0,HT/2
!NEED TO GLUE ENTRY AND EXIT!
FLST,2,12,6,ORDE,4
FITEM,2,1
FITEM,2,-2
!FROM 31 TO 40, IE 10 ITEMS
FITEM,2,31
FITEM,2,-40
VGLUE,P51X
!***MODEL IS NOW BUILT
!
!******************CHANGE THE VIEW TO ISOMETRIC********

/VIEW, 1 ,1,1,1
```

```
/ANG, 1
/REP,FAST
/AUTO, 1
/REP
VPLOT
/COLOR,PBAK,OFF
/REPLOT

!********** CYLINDERS (1/N)*************
LSEL,S,LINE,,16

*DO,I,0,1
*DO,K,0,4
!CYLINDERS EXIT/UPPER SIDE
LSEL,A,LINE,,16 + 1*I + 64*K
!CYLINDERS INLET/LOWER SIDE
LSEL,A,LINE,,56 + 5*I + 64*K
*ENDDO
*ENDDO


*DO,I,0,1
*DO,J,0,1
*DO,K,0,4
!CYLINDERS EXIT/UPPER SIDE
LSEL,A,LINE,,48 + 1*I + 10*J + 64*K
!CYLINDERS INLET/LOWER WALL SIDE
LSEL,A,LINE,,14 + 5*I + 10*J + 64*K
*ENDDO
*ENDDO
*ENDDO

LESIZE,ALL,,,3*H/XD,1/P,,,,1

!************** CYLINDERS (N) ************
LSEL,S,LINE,,15
*DO,I,0,1
*DO,K,0,4
!CYLINDERS INLET/UPPER SIDE
LSEL,A,LINE,,15 + 3*I + 64*K
!CYLINDERS EXIT/LOWER WALL SIDE
LSEL,A,LINE,,55 + 7*I + 64*K
*ENDDO
*ENDDO

*DO,I,0,1
```

```
*DO,J,0,1
*DO,K,0,4
!CYLINDERS INLET/UPPER SIDE
LSEL,A,LINE,,47 + 3*I + 10*J + 64*K
!CYLINDERS EXIT/LOWER WALL SIDE
LSEL,A,LINE,,13 + 7*I + 10*J + 64*K
*ENDDO
*ENDDO
*ENDDO

LESIZE,ALL,,,3*H/XD,1/P,,,,1

!************TEST SECTION SYMMETRY LINES, SHORT***************
LSEL,S,LINE,,321
LSEL,A,LINE,,322
LSEL,A,LINE,,219
LSEL,A,LINE,,220
LSEL,A,LINE,,228
LSEL,A,LINE,,229
LSEL,A,LINE,,281
LSEL,A,LINE,,282
LSEL,A,LINE,,301
LSEL,A,LINE,,302
LSEL,A,LINE,,307
LSEL,A,LINE,,308
LSEL,A,LINE,,365
LSEL,A,LINE,,366
LSEL,A,LINE,,194
LSEL,A,LINE,,199
LSEL,A,LINE,,173
LSEL,A,LINE,,174

*DO,I,0,3
LSEL,A,LINE,,153 + I
LSEL,A,LINE,,327 + I
LSEL,A,LINE,,335 + I
LSEL,A,LINE,,343 + I
LSEL,A,LINE,,351 + I
*ENDDO


LESIZE,ALL,,,H*XD/3,,,,,1

!*****************TEST SECTION SYMMETRY LINES, LONG**************
LSEL,S,LINE,,130
LSEL,A,LINE,,135
```

```
LSEL,A,LINE,,164
LSEL,A,LINE,,165
LSEL,A,LINE,,217
LSEL,A,LINE,,218
LSEL,A,LINE,,237
LSEL,A,LINE,,238
LSEL,A,LINE,,243
LSEL,A,LINE,,244
LSEL,A,LINE,,283
LSEL,A,LINE,,284
LSEL,A,LINE,,292
LSEL,A,LINE,,293
LSEL,A,LINE,,361
LSEL,A,LINE,,362
LSEL,A,LINE,,363
LSEL,A,LINE,,364
LSEL,A,LINE,,179
LSEL,A,LINE,,180

LESIZE,ALL,,,3*H,,,,,1

!***************ENTRY/EXIT SYMMETRY LINES*******************
LSEL,S,LINE,,7
LSEL,A,LINE,,36
LSEL,A,LINE,,90
LSEL,A,LINE,,91

LESIZE,ALL,,,15*H,2,,,,1

!********ENTRY/EXIT SYMMETRY LINES FOR PROPER SPACING**********
LSEL,S,LINE,,71
LSEL,A,LINE,,100
LSEL,A,LINE,,26
LSEL,A,LINE,,27

LESIZE,ALL,,,15*H,1/2,,,,1

!*************INLET AND EXIT LINES******************
LSEL,S,LINE,,2
LSEL,A,LINE,,37
LSEL,A,LINE,,89
LSEL,A,LINE,,92

LESIZE,ALL,,,3*H*SD/XD,,,,,1

!***************GLUE LINES************************
```

```
LSEL,S,LINE,,25
LSEL,A,LINE,,28
LSEL,A,LINE,,3
LSEL,A,LINE,,6
LSEL,A,LINE,,35
LSEL,A,LINE,,38
LSEL,A,LINE,,67
LSEL,A,LINE,,70
LSEL,A,LINE,,99
LSEL,A,LINE,,102
LSEL,A,LINE,,131
LSEL,A,LINE,,134
LSEL,A,LINE,,163
LSEL,A,LINE,,166
LSEL,A,LINE,,195
LSEL,A,LINE,,198
LSEL,A,LINE,,227
LSEL,A,LINE,,230
LSEL,A,LINE,,259
LSEL,A,LINE,,262
LSEL,A,LINE,,66
LSEL,A,LINE,,101

LESIZE,ALL,,,3*H*SD/XD,,,,,1

!*****VERTICAL LINES ENTRY + THOSE NEEDED TO ENSURE PROPER MESH**********
LSEL,S,LINE,,52
LSEL,A,LINE,,45
LSEL,A,LINE,,109
LSEL,A,LINE,,116

LESIZE,ALL,,,V,1/5,,,,1
!**********VERTICAL LINES, TEST SECTION + EXIT***
LSEL,S,LINE,,110
LSEL,A,LINE,,115
LSEL,A,LINE,,51
LSEL,A,LINE,,46

*DO,I,0,1
*DO,K,0,8
LSEL,A,LINE,,10 + 1*I + 32*K
*ENDDO
*ENDDO

!****************VERTICAL LINES (PINS)*****
```

```
*DO,I,0,1
*DO,J,0,1
*DO,K,0,4
LSEL,A,LINE,,21 + 1*I + 10*J + 64*K
LSEL,A,LINE,,53 + 1*I + 10*J + 64*K
*ENDDO
*ENDDO
*ENDDO

LESIZE,ALL,,,V,5,,,,1


LSEL,ALL
ASEL,ALL


!*****************************
!*       BOUNDARY CONDITIONS          *
!*****************************

!*****************PINS VX=VY=VZ=0, T=TWALL*******
ASEL,S,AREA,,9

*DO,K,0,4
*DO,I,0,1
ASEL,A,AREA,,9 + I + 28*K
ASEL,A,AREA,,27 + I + 28*K
*ENDDO
ASEL,A,AREA,,14 +  28*K
ASEL,A,AREA,,23 +  28*K
*ENDDO

DA,ALL,VX,0,1
DA,ALL,VY,0,1
DA,ALL,VZ,0,1
DA,ALL,TEMP,TWALL,1

!*********************ENTRY/EXIT ENDWALLS
VX=VY=VZ=HFLU=0**********
ASEL,S,AREA,,1
ASEL,A,AREA,,12

DA,ALL,VX,0,1
DA,ALL,VY,0,1
DA,ALL,VZ,0,1
SFA,ALL,,HFLUX,0
```

```
!**********************ENDWALL, VX=VY=VZ=0, T=TWALL*****
ASEL,S,AREA,,25
ASEL,A,AREA,,32
ASEL,A,AREA,,49
ASEL,A,AREA,,54
ASEL,A,AREA,,69
ASEL,A,AREA,,77
ASEL,A,AREA,,63
ASEL,A,AREA,,82
ASEL,A,AREA,,91
ASEL,A,AREA,,41
DA,ALL,VX,0,1
DA,ALL,VY,0,1
DA,ALL,VZ,0,1
DA,ALL,TEMP,TWALL,1

!*******SYMMETRY (SIDE) VY=0, HFLU=0 **********
ASEL,S,AREA,,7
ASEL,A,AREA,,24
ASEL,A,AREA,,141
ASEL,A,AREA,,30
ASEL,A,AREA,,45
ASEL,A,AREA,,149
ASEL,A,AREA,,53
ASEL,A,AREA,,60
ASEL,A,AREA,,157
ASEL,A,AREA,,68
ASEL,A,AREA,,73
ASEL,A,AREA,,165
ASEL,A,AREA,,81
ASEL,A,AREA,,88
ASEL,A,AREA,,173
ASEL,A,AREA,,39
ASEL,A,AREA,,16
ASEL,A,AREA,,15
ASEL,A,AREA,,36
ASEL,A,AREA,,40
ASEL,A,AREA,,86
ASEL,A,AREA,,170
ASEL,A,AREA,,80
ASEL,A,AREA,,72
ASEL,A,AREA,,162
ASEL,A,AREA,,67
ASEL,A,AREA,,58
ASEL,A,AREA,,154
```

```
ASEL,A,AREA,,52
ASEL,A,AREA,,44
ASEL,A,AREA,,146
ASEL,A,AREA,,29
ASEL,A,AREA,,22
ASEL,A,AREA,,4

DA,ALL,VY,0,1
SFA,ALL,,HFLUX,0  !HFLUX=HEAT FLUX

!**********SYMMETRY (MIDDLE) VZ=0, HFLU=0******
ASEL,S,AREA,,2
ASEL,A,AREA,,26
ASEL,A,AREA,,35
ASEL,A,AREA,,50
ASEL,A,AREA,,57
ASEL,A,AREA,,64
ASEL,A,AREA,,71
ASEL,A,AREA,,78
ASEL,A,AREA,,85
ASEL,A,AREA,,92
ASEL,A,AREA,,43
ASEL,A,AREA,,13
DA,ALL,VZ,0,1
SFA,ALL,,HFLUX,0

!************INLET VX=VIN VY=VZ=0, T=300K*********
ASEL,S,AREA,,8
DA,ALL,VX,VIN,1
DA,ALL,VY,0,1
DA,ALL,VZ,0,1
DA,ALL,TEMP,300,0

!************EXIT PDOF=0***********
ASEL,S,AREA,,21
DA,ALL,PRES,0,0


ASEL,ALL

!*****************
!*      MESH        *
!*****************

FLST,5,12,6,ORDE,2
FITEM,5,1
```

```
FITEM,5,-12
CM,_Y,VOLU
VSEL, , , ,P51X
CM,_Y1,VOLU                !VOLU=VOLUME, _Y IS USED BY ANSYS
CHKMSH,'VOLU'    !CHECK MESHES
CMSEL,S,_Y                 !S=SELECT A NEW SET,
!*
VSWEEP,ALL                 !_Y1 IS THE VOLUME THAT IS TO BE MESHED BUT
LETS TRY 'ALL'
!*
CMDELE,_Y                  !DELETES A COMPONENT OR ASSEMBLY
CMDELE,_Y1
CMDELE,_Y2
!*
/UI,MESH,OFF


!*****************************************
!*       RUN FIRST (0-20 ITER) SOLUTION        *
!*****************************************
/SOLU
FINISH
/SOLU
SOLVE
!*****************************************
!*       SECOND SOLN (10-20 ITER) OPTIONS   *
!*****************************************
FLDATA1,SOLU,TRAN,0
FLDATA1,SOLU,FLOW,1
FLDATA1,SOLU,TEMP,1
FLDATA1,SOLU,TURB,0
FLDATA1,SOLU,COMP,0
FLDATA1,SOLU,VOF,0
FLDATA1,SOLU,SFTS,0
FLDATA1,SOLU,IVSH,0
FLDATA1,SOLU,SWRL,0
FLDATA1,SOLU,SPEC,0
FLDATA1,SOLU,ALE,0
!*
!*********SECOND EXECUTION CONTROLS*************
/COM,,STEADY STATE ANALYSIS,0
FLDATA2,ITER,EXEC,30,
FLDATA2,ITER,OVER,0,
FLDATA2,ITER,APPE,0,
FLDATA3,TERM,VX,0.01,
FLDATA3,TERM,VY,0.01,
```

```
FLDATA3,TERM,VZ,0.01,
FLDATA3,TERM,PRES,1E-08,
FLDATA3,TERM,TEMP,1E-08,
FLDATA3,TERM,ENKE,0.01,
FLDATA3,TERM,ENDS,0.01,
FLDATA5,OUTP,SUMF,10,
FLDATA5,OUTP,YPLU,T
!**************ADDED TO MAKE DENSITY AN OUTPUT******
FLDATA5,OUTP,DENS,T,
!*
!************SECOND FLUID PROPERTIES ***************
FLDATA12,PROP,DENS,4
FLDATA13,VARY,DENS,1
FLDATA12,PROP,VISC,4
FLDATA13,VARY,VISC,1
FLDATA12,PROP,COND,4
FLDATA13,VARY,COND,1
FLDATA12,PROP,SPHT,4
FLDATA13,VARY,SPHT,1
!*
FLDATA7,PROT,DENS,AIR-SI
FLDATA8,NOMI,DENS,-1
FLDATA9,COF1,DENS,0
FLDATA10,COF2,DENS,0
FLDATA11,COF3,DENS,0
FLDATA7,PROT,VISC,AIR-SI
FLDATA8,NOMI,VISC,-1
FLDATA9,COF1,VISC,0
FLDATA10,COF2,VISC,0
FLDATA11,COF3,VISC,0
FLDATA12,PROP,IVIS
FLDATA7,PROT,COND,AIR-SI
FLDATA8,NOMI,COND,-1
FLDATA9,COF1,COND,0
FLDATA10,COF2,COND,0
FLDATA11,COF3,COND,0
FLDATA7,PROT,SPHT,AIR-SI
FLDATA8,NOMI,SPHT,-1
FLDATA9,COF1,SPHT,0
FLDATA10,COF2,SPHT,0
FLDATA11,COF3,SPHT,0
!*
!*************TEMP CFD SOLVER IS PGMR********************
FLDATA18,METH,TEMP,4,
FLDATA22,MAXI,TEMP,1000,
FLDATA20,SRCH,TEMP,12,
```

```
FLDATA20A,PGMR,FILL,6,
FLDATA20A,PGMR,MODP,0,
FLDATA21,CONV,TEMP,1E-12,
FLDATA23,DELT,TEMP,1E-010,
FLDATA34,MIR,TEMP,0.5,
!*
!**********SECOND ADVECTION PARMS**************
FLDATA,ADVM,MOME,MSU
FLDATA,ADVM,TURB,MSU
FLDATA,ADVM,PRES,MSU
FLDATA,ADVM,TEMP,MSU
!*
!********** RUN SECOND (10-20 ITER) SOLUTION ********
/SOLU
FINISH
/SOLU
SOLVE

!*****************************************************
!*       BEGIN THIRD SOLUTION (20-30 ITER) OPTIONS              *
!*****************************************************
FLDATA1,SOLU,TRAN,0
FLDATA1,SOLU,FLOW,1
FLDATA1,SOLU,TEMP,1
FLDATA1,SOLU,TURB,0
FLDATA1,SOLU,COMP,0
FLDATA1,SOLU,VOF,0
FLDATA1,SOLU,SFTS,0
FLDATA1,SOLU,IVSH,0
FLDATA1,SOLU,SWRL,0
FLDATA1,SOLU,SPEC,0
FLDATA1,SOLU,ALE,0
!*
!*********THIRD EXECUTION CONTROLS*************
/COM,,STEADY STATE ANALYSIS,0
FLDATA2,ITER,EXEC,30,
FLDATA2,ITER,OVER,0,
FLDATA2,ITER,APPE,0,
FLDATA3,TERM,VX,0.01,
FLDATA3,TERM,VY,0.01,
FLDATA3,TERM,VZ,0.01,
FLDATA3,TERM,PRES,1E-08,
FLDATA3,TERM,TEMP,1E-08,
FLDATA3,TERM,ENKE,0.01,
FLDATA3,TERM,ENDS,0.01,
FLDATA5,OUTP,SUMF,10,
```

```
FLDATA5,OUTP,YPLU,T
!*************ADDED TO MAKE DENSITY AN OUTPUT********
FLDATA5,OUTP,DENS,T,
!*
!************THIRD FLUID PROPERTIES *****************
FLDATA12,PROP,DENS,4
FLDATA13,VARY,DENS,1
FLDATA12,PROP,VISC,4
FLDATA13,VARY,VISC,1
FLDATA12,PROP,COND,4
FLDATA13,VARY,COND,1
FLDATA12,PROP,SPHT,4
FLDATA13,VARY,SPHT,1
!*
FLDATA7,PROT,DENS,AIR-SI
FLDATA8,NOMI,DENS,-1
FLDATA9,COF1,DENS,0
FLDATA10,COF2,DENS,0
FLDATA11,COF3,DENS,0
FLDATA7,PROT,VISC,AIR-SI
FLDATA8,NOMI,VISC,-1
FLDATA9,COF1,VISC,0
FLDATA10,COF2,VISC,0
FLDATA11,COF3,VISC,0
FLDATA12,PROP,IVIS
FLDATA7,PROT,COND,AIR-SI
FLDATA8,NOMI,COND,-1
FLDATA9,COF1,COND,0
FLDATA10,COF2,COND,0
FLDATA11,COF3,COND,0
FLDATA7,PROT,SPHT,AIR-SI
FLDATA8,NOMI,SPHT,-1
FLDATA9,COF1,SPHT,0
FLDATA10,COF2,SPHT,0
FLDATA11,COF3,SPHT,0
!*
!***********THIRD ADVECTION PARMS**************
FLDATA,ADVM,MOME,COLG
FLDATA,ADVM,TURB,COLG
FLDATA,ADVM,PRES,COLG
FLDATA,ADVM,TEMP,COLG
!*
!***************RUN THIRD (60-90 ITER) SOLUTION *************
/SOLU
FINISH
/SOLU
```

```
SOLVE

!****************************************
!*        FINAL (90 - MAX ITER) SOLUTION        *
!****************************************

!*********FINAL SOLN OPTIONS*************
FLDATA1,SOLU,TRAN,0
FLDATA1,SOLU,FLOW,1
FLDATA1,SOLU,TEMP,1
FLDATA1,SOLU,TURB,0
FLDATA1,SOLU,COMP,0
FLDATA1,SOLU,VOF,0
FLDATA1,SOLU,SFTS,0
FLDATA1,SOLU,IVSH,0
FLDATA1,SOLU,SWRL,0
FLDATA1,SOLU,SPEC,0
FLDATA1,SOLU,ALE,0
!*
!*********FINAL EXECUTION CONTROLS*************
/COM,,STEADY STATE ANALYSIS,0
FLDATA2,ITER,EXEC,120,
FLDATA2,ITER,OVER,0,
FLDATA2,ITER,APPE,0,
FLDATA3,TERM,VX,0.01,
FLDATA3,TERM,VY,0.01,
FLDATA3,TERM,VZ,0.01,
FLDATA3,TERM,PRES,1E-08,
FLDATA3,TERM,TEMP,1E-08,
FLDATA3,TERM,ENKE,0.01,
FLDATA3,TERM,ENDS,0.01,
FLDATA5,OUTP,SUMF,10,
FLDATA5,OUTP,YPLU,T
!**************ADDED TO MAKE DENSITY AN OUTPUT*******
FLDATA5,OUTP,DENS,T,
!*
!************FINAL FLUID PROPERTIES ****************
FLDATA12,PROP,DENS,4
FLDATA13,VARY,DENS,1
FLDATA12,PROP,VISC,4
FLDATA13,VARY,VISC,1
FLDATA12,PROP,COND,4
FLDATA13,VARY,COND,1
FLDATA12,PROP,SPHT,4
FLDATA13,VARY,SPHT,1
!*
```

```
FLDATA7,PROT,DENS,AIR-SI
FLDATA8,NOMI,DENS,-1
FLDATA9,COF1,DENS,0
FLDATA10,COF2,DENS,0
FLDATA11,COF3,DENS,0
FLDATA7,PROT,VISC,AIR-SI
FLDATA8,NOMI,VISC,-1
FLDATA9,COF1,VISC,0
FLDATA10,COF2,VISC,0
FLDATA11,COF3,VISC,0
FLDATA12,PROP,IVIS
FLDATA7,PROT,COND,AIR-SI
FLDATA8,NOMI,COND,-1
FLDATA9,COF1,COND,0
FLDATA10,COF2,COND,0
FLDATA11,COF3,COND,0
FLDATA7,PROT,SPHT,AIR-SI
FLDATA8,NOMI,SPHT,-1
FLDATA9,COF1,SPHT,0
FLDATA10,COF2,SPHT,0
FLDATA11,COF3,SPHT,0
!*
!**********FINAL ADVECTION PARMS**************
FLDATA,ADVM,MOME,COLG
FLDATA,ADVM,TURB,COLG
FLDATA,ADVM,PRES,COLG
FLDATA,ADVM,TEMP,COLG
!*
!*****************RUN FINAL SOLUTION************
/SOLU
FINISH
/SOLU
SOLVE

!************************
!*        POST PROCESSING *
!************************

!********************MAKE IT GO TO LAST SET*****************
/POST1
FINISH
/POST1
SET,LAST
!*********************ADD DENSITY*******************************

!! RETREIVES (TEMP, VELOCITY, HEAT FLUX
```

```
!!              FILM COEFFICIENT, AND NODAL-XCOORD) FROM THE ANSYS
MODEL

/POST1
!! DEFINE ARRAYS
*GET,MAXNODE,NODE,0,COUNT
*DIM,DENSITY,,MAXNODE,1

!! FILL ARRAYS
*DO,I,1,MAXNODE
*GET,DENSITY(I,1),NODE,I,DENS
*ENDDO

!! SEND ARRAYS TO YOUR LOCAL DRIVE
*CFOPEN,DENSITY,TXT
*VWRITE,DENSITY(1,1)
(F10.4)

!**************************GETDATA*******************************
***
!! RETREIVES (TEMP, VELOCITY, HEAT FLUX,
!!         NODAL-XCOORD, NODAL-YCOORD, NODAL-ZCOORD,
!!         PRESSURE AND FILM COEFFICIENT) FROM THE ANSYS MODEL

/POST1
!! DEFINE ARRAYS
*GET,MAXNODE,NODE,0,COUNT
*DIM,ANRES,,MAXNODE,8

!! FILL ARRAYS
*DO,I,1,MAXNODE
*GET,ANRES(I,1),NODE,I,TEMP
*GET,ANRES(I,2),NODE,I,V,X
*GET,ANRES(I,3),NODE,I,HFLU
*GET,ANRES(I,4),NODE,I,LOC,X
*GET,ANRES(I,5),NODE,I,LOC,Y
*GET,ANRES(I,6),NODE,I,LOC,Z
*GET,ANRES(I,7),NODE,I,PRES
*GET,ANRES(I,8),NODE,I,HFLM
*ENDDO

!! SEND ARRAYS TO YOUR LOCAL DRIVE
*CFOPEN,ANRES,TXT
*VWRITE,SEQU,ANRES(1,1),ANRES(1,2),ANRES(1,3),ANRES(1,4),ANRES(1,5),A
NRES(1,6),ANRES(1,7),ANRES(1,8)
(F7.0, 3F10.2, 3F10.5, 2F10.2)
```

```
!********************NODES*****************
/PREP7
!ROW 1
ASEL,S,AREA,,9
ASEL,A,AREA,,10
ASEL,A,AREA,,14
NSLA,S,0
NWRITE, ROW1,TXT

!ROW 2
ASEL,A,AREA,,23
ASEL,A,AREA,,27
ASEL,A,AREA,,28

NSLA,S,0
NWRITE, ROW2,TXT

!ROW 3
ASEL,A,AREA,,37
ASEL,A,AREA,,38
ASEL,A,AREA,,42
NSLA,S,0
NWRITE, ROW3,TXT

!ROW 4
ASEL,A,AREA,,51
ASEL,A,AREA,,55
ASEL,A,AREA,,56

NSLA,S,0
NWRITE, ROW4,TXT

!ROW 5
ASEL,A,AREA,,65
ASEL,A,AREA,,66
ASEL,A,AREA,,70

NSLA,S,0
NWRITE, ROW5,TXT

!ROW 6
ASEL,A,AREA,,79
ASEL,A,AREA,,83
ASEL,A,AREA,,84
NSLA,S,0
```

```
NWRITE, ROW6,TXT

!ROW 7
ASEL,A,AREA,,93
ASEL,A,AREA,,94
ASEL,A,AREA,,98
NSLA,S,0
NWRITE, ROW7,TXT

!ROW 8
ASEL,A,AREA,,107
ASEL,A,AREA,,111
ASEL,A,AREA,,112
NSLA,S,0
NWRITE, ROW8,TXT

!ROW 9
ASEL,A,AREA,,121
ASEL,A,AREA,,122
ASEL,A,AREA,,126
NSLA,S,0
NWRITE, ROW9,TXT

!ROW 10
ASEL,A,AREA,,135
ASEL,A,AREA,,139
ASEL,A,AREA,,140
NSLA,S,0
NWRITE, ROW10,TXT

!ENDWALL
ASEL,S,AREA,,25
ASEL,A,AREA,,32
ASEL,A,AREA,,49
ASEL,A,AREA,,54
ASEL,A,AREA,,69
ASEL,A,AREA,,77
ASEL,A,AREA,,63
ASEL,A,AREA,,82
ASEL,A,AREA,,91
ASEL,A,AREA,,41
NSLA,S,0
NWRITE,ENDWALL,TXT
```

APPENDIX B. EQUATIONS

The equation formulation and constant parameters used are further illustrated in this Appendix. The equations were coded in to a Microsoft excel spreadsheet. The results obtained from the numerical solutions were then entered into this spreadsheet so that the computational results can be compared with the theoretical solutions.

Constants used for the numerical solutions

Total number of pins	N_{pins}	15	
Inlet Temperature	T_{inlet}	300	[K]
Temperature for end wall of test section	T_{wall}	306	[K]
Film Temperature	T_{film}	303	[K]
Reference Temperature	T_0	273.15	[K]
Reference Coeff of viscosity	μ_0	0.0000171	[N.s/m^2]
Coeff of viscosity (Based on T_{flim})	μ	1.85357E-05	[N.s/m^2]
Reference Pressure	P_{ref}	101350	[Pa]
Inlet Density @T_{in}=300	ρ_{in}	1.177119628	[kg/m^3]
Inlet Density @T_{flim}	ρ_{film}	1.165464979	[kg/m^3]
Kinematic Viscosity (Based on T_{flim})	υ	1.59042E-05	[m^2/s]
Thermal Conductivity	k	2.64E-02	[W/m]

Equations

$$\text{Film Temperature, } T_{film} = \frac{T_{inlet} + T_{wall}}{2} \qquad \text{------- (1)}$$

Coefficient of viscosity (based on Tfilm), Sutherland Law

$$\left.\begin{aligned} \frac{\mu}{\mu_o} &= \left(\frac{T}{T_o}\right)^{\frac{3}{2}} \frac{T_o + S_{air}}{T + S_{air}} \\ \mu &= \mu_o \left(\frac{T}{T_o}\right)^{\frac{3}{2}} \frac{T_o + S_{air}}{T + S_{air}} \end{aligned}\right\} \begin{aligned} &\text{reference viscosity, } \mu_o = 1.71\text{x}10^{-5} \text{ kg/ms} \\ &\text{reference temperature, } T_o = 273.15 \text{ K} \\ &\text{Constant, } S_{air} \text{ for air} = 110.4^{o}\text{K} \end{aligned} \qquad \text{--- (2)}$$

$$\text{Density at } T_{in},\ \rho_{in} = \frac{P_{ref}}{(287)(T_{in})} \qquad \text{------ (3)}$$

Density at T_{film}, $\rho_{film} = \frac{P_{ref}}{(287)(T_{film})}$ ------ (4)

Viscosity (based on T_{film}), $\nu = \frac{\mu}{\rho_{film}}$ ------ (5)

Length / streamwise distance, $X = \left(\frac{X}{D}\right)(D)$ ------ (6)

Spanwise distance, $S = \left(\frac{S}{D}\right)(D)$ ------ (7)

Height distance, $H = \left(\frac{H}{D}\right)(D)$ ------ (8)

Theoretical outlet temperature

This is to verify the theoretical outlet temperature with numerical value.

Outlet Bulk Temperature, $T_{bulk,out} = T_{bulk,in} + \frac{Q}{\dot{m}\, C_p}$ ------ (9)

Face Area

$A_{Face} = (1.5 * S) * (10 * X)$ ----- (10)

Wetted area

The wetted area is defined as:

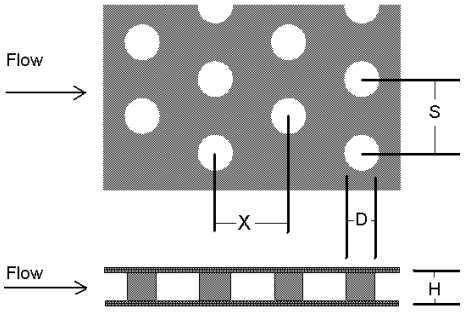

Schematic of a staggered pin-fin array

$$A_{wetted} = A_{wpin} + 2\left(A_{Face} - 15\pi\frac{D^2}{4}\right)$$

$$= 15\pi DH + 2\left(A_{Face} - 15\pi\frac{D^2}{4}\right) - - - (11)$$

Array volume

$$V_{array} = (1.5 * S) * (10 * X) * H \text{ ----- (12)}$$

Open array volume

Open array volume, $V_{array,open}$ is defined as:

$$V_{array,open} = V_{array} - V_{pins}$$

$$= (\#\text{ of cells spanwise} \times S)(\#\text{ of cells lengthwise} \times X)(H) - \left(N_{pins}\pi\frac{D^2}{4}H\right)$$

$$= (1.5S)(10X)(H) - \left(15\pi\frac{D^2}{4}H\right) \quad - - - - (13)$$

Average Area

$$\overline{A} = \frac{V_{array,open}}{L} = \frac{V_{array,open}}{(10)(X)} \quad \text{------- (14)}$$

Hydraulic diameter

$$D_h = \frac{4V_{open}}{A_{wetted}} \quad \text{------ (15)}$$

Calculation based on a unit cell

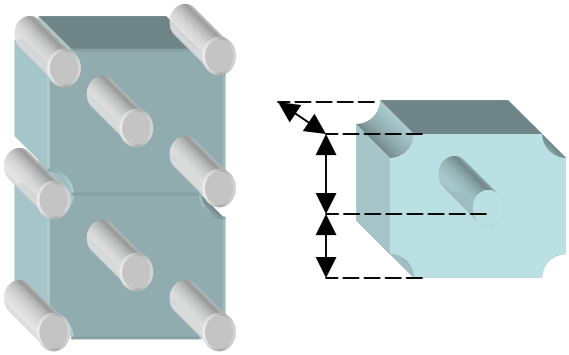

Open volume per unit cell

$$V_{open,uc} = (S)(2X)(H) - \left(2H\pi\frac{D^2}{4}\right) \quad \text{--------- (16)}$$

Wetted area per unit cell

$$A_{wetted,uc} = (2\pi D)(H) + 2\left[(S)(2X) - 2\pi\left(\frac{D^2}{4}\right)\right] \quad \text{-------- (17)}$$

Average Area of the inlet per unit cell

$$\bar{A}_{uc} = \frac{V_{open,uc}}{2X} \quad \text{--------- (18)}$$

Nominal inlet area of the duct per unit cell

Area of the inlet duct per unit cell, A_{duct} is

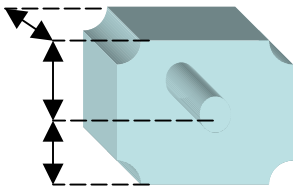

$$A_{duct,uc} = 2\left(\frac{s}{2}\right)h = s \times h \quad \text{----- (19)}$$

Hydraulic diameter per unit cell

$$D_{h,uc} = \frac{4V_{open,uc}}{A_{wetted,uc}} \quad \text{-------- (20)}$$

Inlet velocity

$$Re_{D_h} = \frac{\left(\rho_{T=300} U_{in} A_{duct,uc}\right) D_{h,uc}}{\overline{A}_{uc}\mu}$$

$$U_{in} = \frac{Re_{D_h}\,\overline{A}_{uc}\mu}{\rho_{T=300} A_{duct,uc} D_{h,uc}} ----(21)$$

Average velocity

$$U_{avg} = \frac{\dot{m}}{(\rho_{film})(\overline{A})} \qquad \text{-------- (22)}$$

Entry hydraulic diameter

The entry hydraulic diameter of a wide channel is twice the distance between the plates.

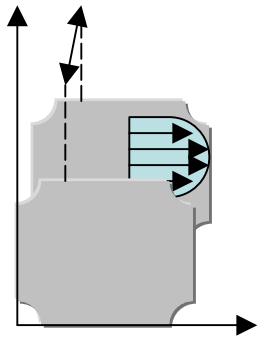

Entry hydraulic diameter

$$D_{h,entry} = \frac{4 \times \text{cross-sectional area}}{\text{wetted perimeter}} = \lim_{S\to\infty} \frac{4(S \times H)}{2S + 2H} = 2H$$

$$D_{h,entry} = 2h \quad \text{------ (23)}$$

Entry Reynolds number

$$\text{Entry Reynolds numbers, } Re_{Dh,entry} = \frac{U_{in} D_{h,entry}}{\nu} \qquad \text{----- (24)}$$

Entrance Length (for laminar flow)

For laminar flow, the accepted correlation for entrance length, L_e is

$$\frac{L_e}{D_{h,entry}} \approx 0.06\,Re_{h,entry}$$

$$L_e \approx 0.06\left(D_{h,entry}\right)\left(Re_{h,entry}\right) \quad ----(25)$$

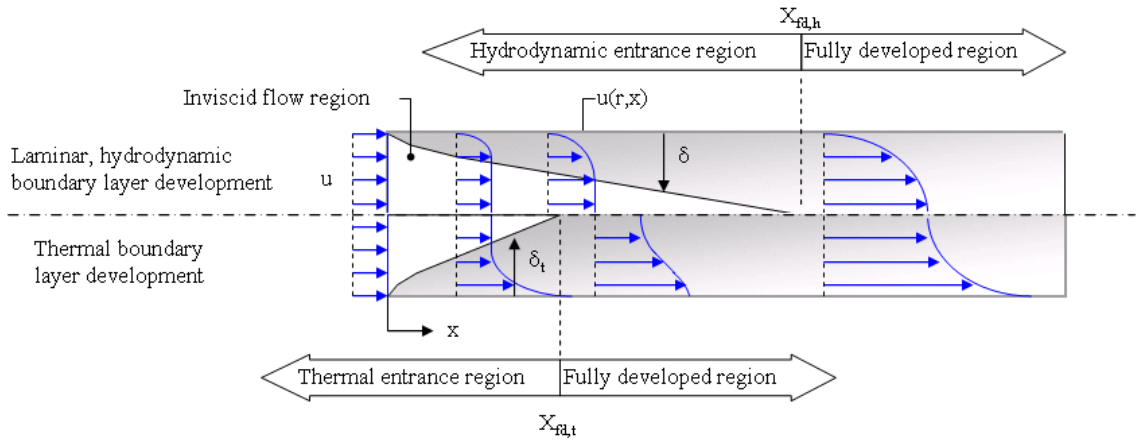

Log mean temperature

$$\Delta T_{lm} = \frac{\left(T_{wall} - T_{bulk,out}\right) - \left(T_{wall} - T_{bulk,in}\right)}{\ln\left(\frac{T_{wall} - T_{bulk,in}}{T_{wall} - T_{bulk,out}}\right)} \quad ---------- (26)$$

Array average heat transfer coefficient

$$\bar{h}_{array} = \frac{Q}{A_{wetted}\,\Delta T_{lm}} \quad -------- (27)$$

Nusselt number

$$Nu_{D_h} = \frac{\left(\bar{h}_{array}\right)\left(D_h\right)}{k} \quad ------- (28)$$

Pressure Gradient and Friction Factor in Fully Developed Flow

Friction factor for laminar duct, $f_{duct,lam} = \frac{96}{Re_{D_h,entry}}$ ------- (29)

Friction head loss, $h_f = f_{duct,lam} \frac{L}{D_h} \frac{U_{in}^2}{2g}$ where L is total length for entry and exit duct

Duct Pressure, $\Delta P_{duct} = \rho g h_f$

$$= \rho g \left(f_{duct,lam} \frac{L}{D_{h,entry}} \frac{U_{in}^2}{2g} \right)$$

$$= \frac{\rho f_{duct,lam} U_{in}^2 L}{2 D_{h,entry}} \qquad \text{------- (30)}$$

$$\Delta P_{array} = \Delta P_{num} - \Delta P_{duct} \qquad \text{------- (31)}$$

where ΔP_{num} is the pressure drop across the duct and array obtained from ANSYS result.

Therefore,

Friction factor of the array, $f = \frac{\Delta P_{array} D_h}{\frac{1}{2} \rho U_{avg}^2 L_{test\ sect}}$

$$= \frac{\Delta P_{array} D_h}{\frac{1}{2} \rho U_{avg}^2 (10X)} \qquad \text{------- (32)}$$

Perform Check

Reynolds Number based on Hydraulic Diameter

$$Re_{D_h} = \frac{\rho u_m D_h}{\mu}$$

$$= \frac{\dot{m}_{in} D_h}{\bar{A}_{uc} \mu} \qquad \text{where } \dot{m}_{in} = \rho u_{in} A_{duct,uc} \qquad \text{------ (33)}$$

Effective heat transfer coefficient

$$\bar{h}_{eff} = \frac{Q}{2 A_{face} \Delta T_{lm}}$$

Effective Nu

$$Nu_{eff} = \frac{\left(\bar{h}_{eff}\right)\left(D_h\right)}{k}$$

LIST OF REFERENCES

Ref. 1 VanFossen, G.J., "Heat Transfer Coefficient for Staggered Arrays of Short Pin Fins," ASME *J. of Engineering for Power*, Vol. 104, pp. 268-274, 1982.

Ref. 2 Sparrow, E.M., Stahl, T.J., and Traub, P., "Heat Transfer Adjacent to the attached end of a Cylinder in Crossflow," *Int. J. of Heat and Mass Transfer*, Vol. 25, pp. 233-242, 1984.

Ref. 3 Chyu, M.K., Hsing, Y.C., Shih, T. I.-P., and Natarajan, V., "Heat Transfer Contributions of Pins and Endwall in Pin-Fin Arrays: Effects of Thermal Boundary Condition Modeling," *ASME J. of Turbomachinery*, Vol. 121, pp. 257-263, 1998.

Ref. 4 Metzger, D.E., Berry, R.A., Bronson, J.P., "Developing Heat Transfer in Rectangular Ducts With Staggered Arrays of Short Pin Fins", ASME *J. of Heat Transfer*, Vol. 104, pp. 700-706, 1982.

Ref. 5 Donahoo, E.E., Camci, C., Kulkarni, A.K., and Belegundu, A.D., "Determination of Optimal Row Spacing for a Staggered Cross-Pin Array in a Turbine Blade Cooling Passage," *Enhanced Heat Transfer*, Vol. 8, pp. 41-53, 2001.

Ref. 6 Hamilton, L.J., *Numerical Analysis of the Performance of a Staggered Cross-Pin Array Heat exchanger*, Naval Postgraduate School, Monterey, California, 2003.

Ref. 7 "ANSYS Documentation", [http://www1.ansys.com/customer/],

Ref. 8 Kays, W.M. and London, A.L., *Compact Heat Exchangers*, 3rd Ed., McGraw-Hill, New York, 1984.

Ref. 9 Frank P. Incropera, David P. Dewitt, *Introduction to Heat Transfer,* , pp. 434-473, John Wiley & Sons, 2001.

Ref. 10 White, F. M., *Fluid Mechanics*, McGraw-Hill, Inc., 4th Ed., 1999.

Ref. 11 "*MEMS Heat Exchangers for Harsh Environments*", DARPA, http://me.lsu.edu/~ekkad/research.html, June 2003.

INITIAL DISTRIBUTION LIST

1. Defense Technical Information Center
   Ft. Belvoir, Virginia

2. Dudley Knox Library
   Naval Postgraduate School
   Monterey, California

3. Chairman and Associate Professor Ashok Gopinath
   Naval Postgraduate School
   Monterey, California

4. CPT Jui Sheng Choo, Singapore Army
   Naval Postgraduate School
   Monterey, California